PUBLICACIONS

Aquesta Tesi es presenta en la modalitat de compendi de publicacions. El recull d'articles ja publicats que ha donat lloc a aquest treball és:

Comunicació A: Isolation of Two Regioisomers of a Triad of C_{60} Based on a Tetrathiafulvalene Derivative. HMBC NMR as a Useful Tool for their Characterisation

M. Mas-Torrent, M. Pons, M.A. Molins, J. Veciana and C. Rovira.

Synth. Met., 123, 523-527 (2001).

Article B: Isolation and Characterization of Four Isomers of a C_{60} Bisadduct with a TTF Derivative. Study of their Radical Ions.

M. Mas-Torrent, R. Rodríguez-Mias, M. Solà, M. A. Molins, M. Pons, J. Vidal-Gancedo, J. Veciana and C. Rovira.

J. Org. Chem., 67, 566-575 (2002).

Comunicació C: A New Family of Conducting and Magnetic Charge-Transfer Salts from BMDT-TTF.

M. Mas-Torrent, S. S. Turner, K. Wurst, J. Vidal-Gancedo, J. Veciana, P. Day, C. Rovira.

Synth. Met., 120, 799-800 (2001).

Article D: New Flexible Low Density Metallic Materials Containing the (BEDT-TTF)$_2$(I_xBr_{1-x})$_3$ Molecular Metals as Active Components.

E. Laukhina, V. Tkacheva, I. Chuev, E. Yagubskii, J. Vidal-Gancedo, M. Mas-Torrent, C. Rovira, J. Veciana, S. Khasanov, R. Wojciechowski J. Ulanski.

J. Phys. Chem. B, 105, 11089-11097 (2001).

Article E: New transparent metal-like bi-layer composite films with high conducting layers of the θ-(BET-TTF)$_2$Br3H_2O nanocrystals.

M. Mas–Torrent, E. Laukhina, C. Rovira, J. Veciana, V. Tkacheva, L. Zorina and S. Khasanov.

Adv. Funct. Mater., 11, 4, 299-303 (2001).

COMUNICACIÓ A

Títol: Isolation of Two Regioisomers of a Triad of C_{60} Based on Tetrathiafulvalene Derivative. HMBC NMR as a Useful Tool for their Characterisation.

Autors: M. Mas-Torrent, M. Pons, M.A. Molins, J. Veciana and C. Rovira.

Publicació: *Synth. Met.*, 123, 523-527

Any: 2001

ELSEVIER

Synthetic Metals 123 (2001) 523–527

SYNTHETIC METALS

www.elsevier.com/locate/synmet

Isolation of two regioisomers of a triad of C_{60} based on a tetrathiafulvalene derivative HMBC NMR as a useful tool for their characterisation

M. Mas-Torrent[a], M. Pons[b], M.A. Molins[c], J. Veciana[a], C. Rovira[a,*]

[a]*Institut de Ciència de Materials de Barcelona (CSIC), Campus Universitari, 08193 Bellaterra, Spain*
[b]*Departament de Química Orgànica, Facultat de Química, Universitat de Barcelona, Martí i Franqués 1, 08028 Barcelona, Spain*
[c]*Serveis Cientificotècnics, Lluís Solé i Sabarís, 08028 Barcelona, Spain*

Received 15 January 2001; received in revised form 28 February 2001; accepted 3 March 2001

Abstract

A family of triads formed by C_{60} and two identical addends of a TTF derivative has been synthesised and two of the resulting isomers isolated and characterised. HMBC NMR provides a powerful means of characterising C_{60} dyads and triads as it is much more sensitive than ^{13}C NMR. With this technique further information can be obtained such as the differentiation and assignment of the same kind of nucleus or the identification of Csp^2 fullerene cage carbons. © 2001 Elsevier Science B.V. All rights reserved.

Keywords: Fullerenes and derivatives; Nuclear magnetic resonance spectroscopy; UV–VIS–NIR absorption; Mass spectroscopy

1. Introduction

Polyadducts of C_{60} with well-defined three-dimensional structure are of great importance as they reveal intrinsical biological [1] or material properties [2,3]. Up to now, several electron donors such as porphyrins, ferrocene, tetrathiafulvalenes or phtalocyanines have been attached to the fullerene cage [3–22] and, in some cases, the final compounds show interesting intramolecular electronic interactions between the C_{60} and the addends. Some of these donor–acceptor dyads form long-lived charge separated species upon irradiation [12–22], being interesting systems as molecular building blocks in electrooptical devices and bistable molecular information storage units.

On the other hand, and despite the fact that there are not many precedents due to the strenuous work required for the isolation and characterisation of the isomers, the synthesis of triads ($C_{60}R_2$) is of great interest for studying the influence of the isomerism on the physical properties [23–29]. As crystals of these compounds suitable for X-Ray structure determination are usually difficult to obtain [30], the attribution of the correct structure for all the isomers has become an important aim to achieve and several groups have been recently working in finding a systematic method to characterise them. Hirsch and co-workers established an empirical rule that consists in a combination of polarity criteria, NMR and UV–VIS spectroscopic data [26]. Wilson and Schuster and co-workers have also attempted to correlate the structure of the bisadducts with the ^3He chemical shifts in the NMR spectra of $^3He@C_{60}$ fullerene derivatives [24]. More recently, Pasimeni et al. suggested a new method based on an EPR study of the excited triplet state of the bisadducts [28]. The ^1H NMR and ^{13}C NMR spectra are also a helpful tool to identify fullerene bisadducts. In fact, *trans*-1 and *e* isomers can be assigned unambiguously by NMR using symmetry considerations. However, only the C-bridges between the addend and the C_{60} can be assigned and it is not possible either to differentiate the rest of the isomers. Moreover, the method is very insensitive due to the low solubility of this kind of compounds and the long relaxation times of C_{60} carbons.

In this paper, we report on the isolation and characterisation of two of the isomers of a family of triads $C_{60}(TTF)_2$. We will also show that HMBC spectra (Heteronuclear Multiple Bond Correlation) [31] provide a sensitive method to characterise fullerene derivatives with protonated addends. In HMBC spectra, carbon magnetisation is indirectly detected via two- or three-bond couplings to the substituent protons. The increased sensitivity derives from polarisation transfer from protons and the use of shorter

* Corresponding author. Fax: +34-935805729.
E-mail address: cun@icmab.es (C. Rovira).

0379-6779/01/$ – see front matter
PII: S0379-6779(01)00348-4

recycle times during signal accumulation, dictated by the fast relaxing protons.

2. Results and discussion

Previously, a new family of C_{60}TTF cyclohexene-fused dyads were synthesised in our group, in which the derived transient charge-separated open-shell species show a very long lifetime [18]. Thus, the study of the triad **1** formed by two identical TTF's attached to C_{60} (Chart 1) is very interesting and the synthesis has been carried out either by direct Diels–Alder bisaddition of the diene generated upon loss of SO_2 of bis(methoxycarbonyl)-3-sulfolene-tetrathiafulvalene to the C_{60} [18], or by further cycloaddition of the monoadduct **2** (Scheme 1). Depending on the relative position of the addends in the cage, eight regioisomers can be formed (Chart 1), which were detected by analytical HPLC on silica gel as stationary phase (Fig. 1). Further separation with a semi-preparative column of the very insoluble mixture of regioisomers provided in milligram quantities two of the isomers **1a** and **1e**, which correspond to the first and the fifth peak of the chromatogram. The laser desorption and ionisation time of flight (LDI-TOF) mass spectra of them show the molecular peak at *m*/*z* 1412 which confirms that they are isomers of **1**. Taking into account the polarity considerations and comparing the obtained UV–VIS spectra of them in the region between 400 and 800 nm (Fig. 2), which is characteristic of the addition pattern, with the ones found for other C_{60} bisadducts [23,26], the isomers **1a** and **1e** can be tentatively assigned to the isomers *trans*-2 and *e*, respectively. Despite the fact that good NMR spectra were not possible to obtain due to the very low solubility of these compounds, thanks to the use of the HMBC technique their NMR characterisation has been possible, which is in good agreement with the previous assignation of the isomers. These simple spectra usually allow the study of an isomer even in mixtures or in the presence of impurities. The HMBC spectra characterise each isomer according to its symmetry properties.

The monoadduct **2** was first studied by HMBC NMR as a model system. Resolved by the frequencies of the addend carbons, this spectrum contains the correlation of the methyl protons (H_B) with the carbonilic carbons, the two-bond

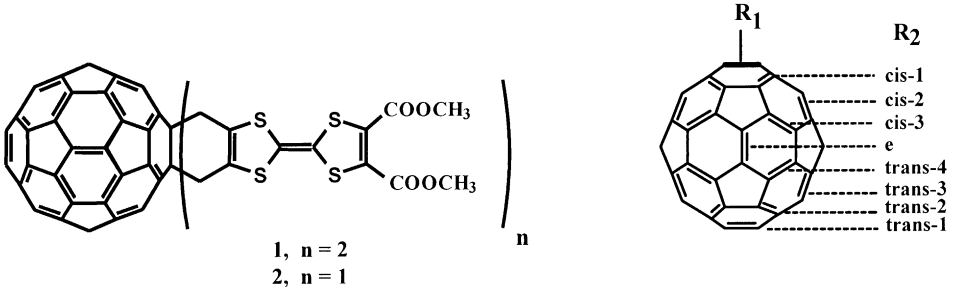

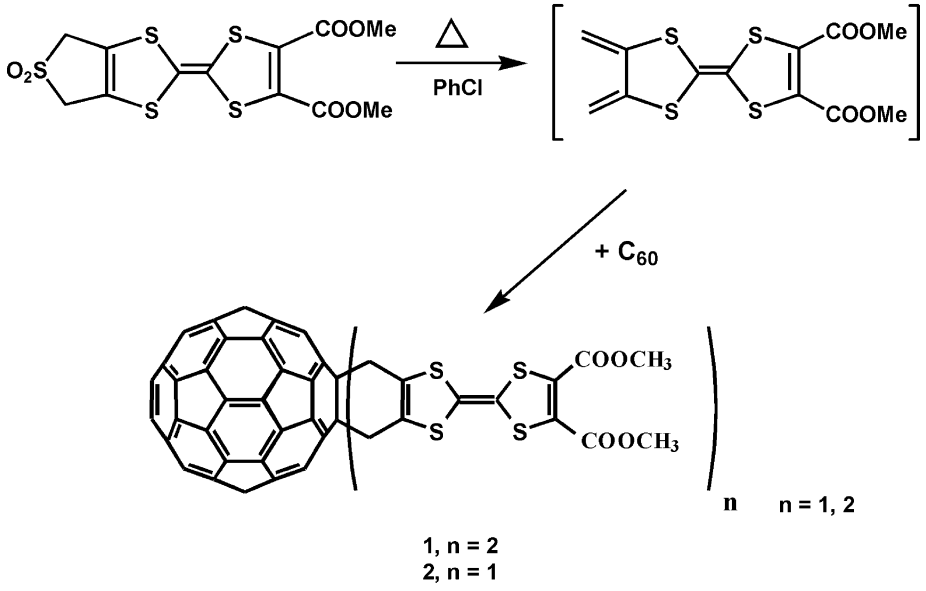

Scheme 1.

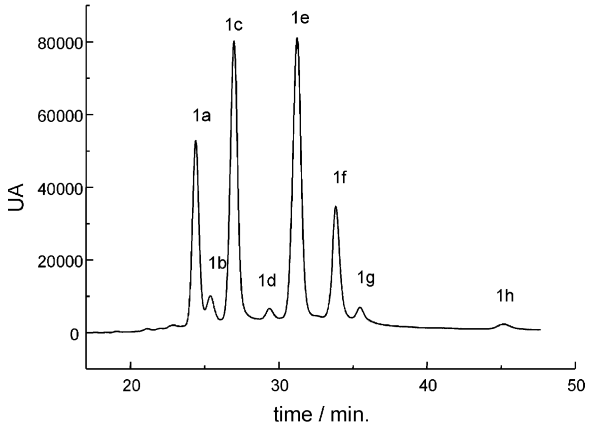

Fig. 1. HPLC chromatogram of the mixture of isomeric bisadducts of **1**. Conditions: 25 cm × 0.46 cm Spherisorf Silica column, 0.3 % AcOEt in CH_2Cl_2 (1 ml/min), UV–VIS detection at 290 nm.

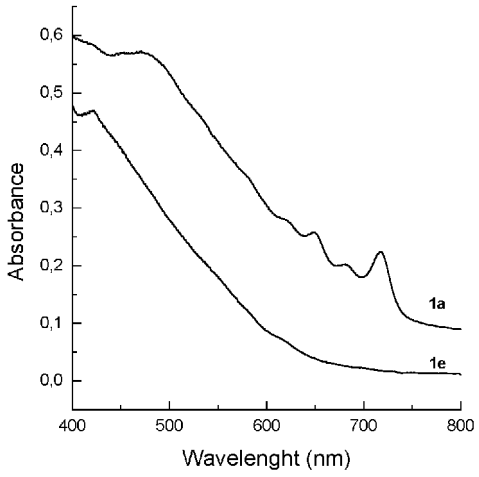

Fig. 2. UV–VIS spectra of isomers **1a** and **1e** in CH_2Cl_2.

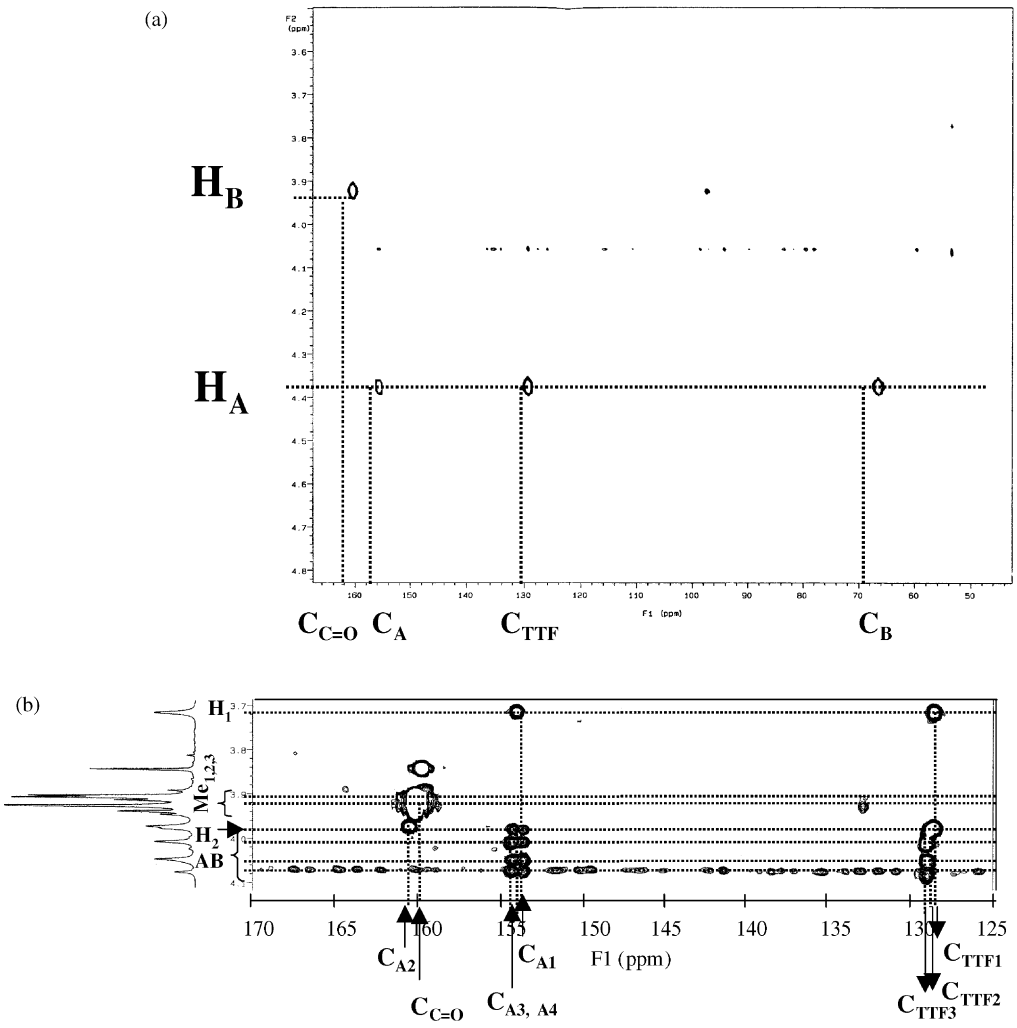

Fig. 3. (a) HMBC spectrum of monoadduct **2**. (b) HMBC spectrum of the equatorial bisadduct **1e**.

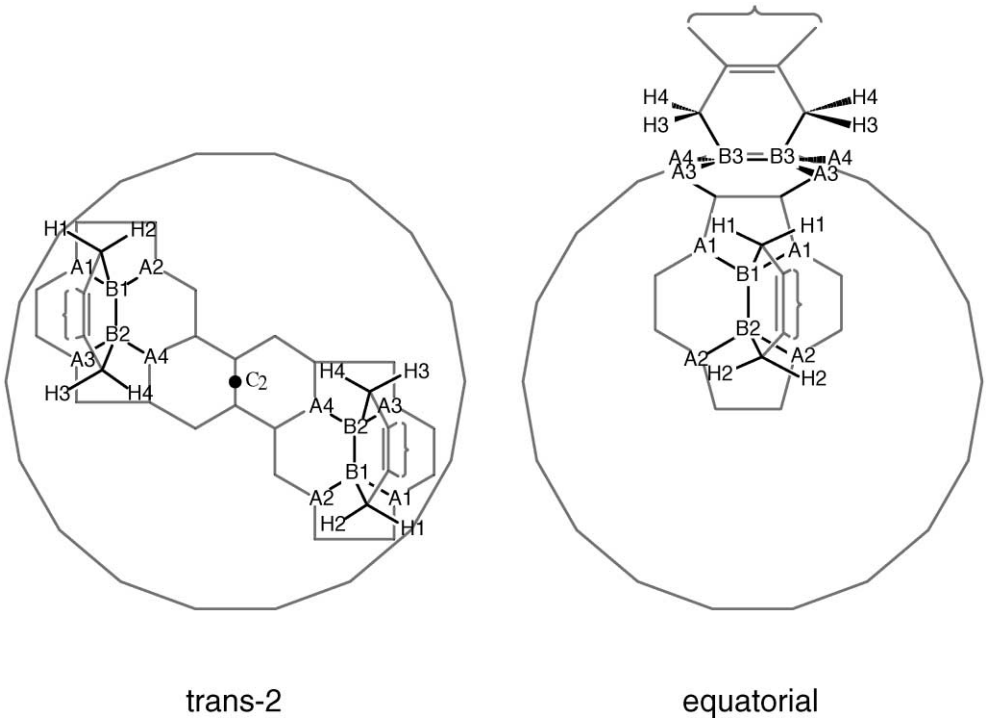

Fig. 4. Diagnostic proton and carbon resonances of equatorial and *trans*-2 isomers of triad **1** detected in HMBC spectra. Equatorial isomer. ^{1}H-NMR: 3.72 (s, H1), 3.98 (s, H2), 4.02–4.06 (AB, 15 Hz, H3–H4) ^{13}C-NMR: 65.6 (B1), 65.2 (B2), 65.2 (B3), 154 (A1), 161 (A2), 153.5 (A3), 154.5 (A4). *Trans*-2 isomer. ^{1}H-NMR: 4.40–4.60 (AB, 15 Hz, H1–H2), 4.35–4.40 (AB, 15 Hz, H3–H4) ^{13}C-NMR: 65.0 (B1), 64.5 (B2), 153.6 (A1), 154.4 (A2), 153.8 (A3), 160.0 (A4). The number of additional signals from TTF carbons and methyl protons, observed in all these isomers, are in agreement with their respective symmetries.

coupling of the methylene protons (H_A) with the Csp^2 of the TTF (C_{TTF}) and the bridge carbons of the fullerene (C_B) and the three-bond coupling to the adjacent carbons (C_A) (Fig. 3a). Some Csp^2 cage carbons of some C_{60} derivatives were previously tentatively assigned by ^{13}C NMR [32] and, very recently, the use of INADEQUATE 2D NMR experiments have allowed the complete assignment of a tethered fullerene bisadduct [33]. However, while these techniques require a reasonable amount of sample or ^{13}C enriched samples, here we have been able to assign unambiguously some of the sp^2 carbons of the fullerene cage using only 1–2 mg of sample. This information is specially useful for the analysis of the isomers of bisadduct **1**, or in general, for studying C_{60} derivatives which are difficult to obtain or those which are very insoluble.

In agreement with the symmetry of equatorial bisadduct **1e**, we observe the methylenic protons of one of the addends as an AB system and those from the other one, as two A_2 singlets. The unexpected low frequency of one of them has been attributed to ring currents of the π system of the other TTF, and allows its assignment to protons H_1 (Fig. 4). The standard ^{13}C-NMR spectrum shows the expected three different C_B carbons. The HMBC spectra in addition allow the observation of four different C_A and three of the sp^2 TTF carbons. (Figs. 3b and 4). The C_{A2} carbon, which correlates with the singlet proton at 3.98 ppm, resonates at ca. 160 ppm, >6 ppm higher than the other adjacent carbons. Unassigned carbons at this frequency had previously been observed in other equatorial isomers [28,29].

The *trans*-2 isomer **1a** has a binary symmetry axis that renders the two TTF groups equivalent, but nuclei within each TTF group are non-equivalent (Fig. 4). Thus, the methylenic protons are observed as two AB systems. On the other hand, there are two different C_B carbons, four C_A and four C_{TTF}. As in the case of the equatorial isomer, one of the C_A also appears at 160.0 ppm. No cage resonances at this frequency were observed either in the reported *cis*-3 or *trans*-4 isomers of other bisadducts or in the monoadducts [23–29]. It is worth pointing out that in *trans*-2 and *equatorial* isomers, the relative disposition of the anomalous C_A with respect to the anchoring bond of the second TTF addend, along a pathway defined by two connected 5-radialene units, is the same.

3. Conclusions

To conclude, a family of $C_{60}(TTF)_2$ triads has been synthesised and two of the isomers isolated. The HMBC has been proved to be a useful tool to characterise them, which has permitted us to assign unambiguously the chemical shifts of some C_{60} sp^2 carbons using very small amounts of sample. If the observation that some adjacent carbons appear at an unexpected chemical shift only in

some of the isomers, can be generalised, it may provide an additional simple tool for the characterisation of C_{60} bisadducts.

Acknowledgements

This work was supported from DGES (BQU200-1157 and PB97-0933) and CIRIT (2000 SGR 00114). M. Mas-Torrent is grateful to the Generalitat de Catalunya for a pre-doctoral grant.

References

[1] S.H. Friedman, D.L. De Camp, R.P. Sijbesma, G. Srdanov, F. Wudl, G.L. Kenyon, J. Am. Chem. Soc. 115 (1993) 6506.
[2] A. Hirsch, Adv. Mater. 5 (1993) 859.
[3] M. Prato, J. Mater. Chem. 7 (1997) 1097.
[4] Y. Rubin, S. Khan, D.I. Freedberg, C. Yeretzian, J. Am. Chem. Soc. 115 (1993) 344.
[5] Y. Rubin, S.I. Khan, A.M. Oliver, M.N. Paddon-Row, J. Am. Chem. Soc. 115 (1993) 4919.
[6] K. Mullen, P. Belik, A. Gügel, J. Spickermann, Angew. Chem. Int. Ed. Engl. 32 (1993) 78.
[7] P. Liddell, A.N. Mcpherson, J. Sumida, L. Demanche, A.L. Moore, T.A. Moore, D. Gust, Photochem. Photobiol. 595 (1994) 365.
[8] T.G. Linssen, K. Dürr, M. Hannack, A. Hirsch, J. Chem. Soc., Chem. Commun. (1995) 103.
[9] Y. Matsubara, H. Tada, S. Nagase, Z. Yoshida, J. Org. Chem. 60 (1995) 5372.
[10] L. Isaacs, T.G. Haldimann, F. Diederich, Angew. Chem. Int. Ed. Engl. 33 (1994) 22, 2339.
[11] C. Boulle, J.-M. Rabreau, P. Hudhomme, M. Cariou, M. Jubault, A. Gorgues, J. Orduna, J. Garín, Tetrahedron Lett. 38 (1997) 3909.
[12] H. Imahori, Y. Sakata, Adv. Mater. 9 (1997) 537.
[13] N. Martín, L. Sánchez, B. Illescas, I. Pérez, Chem. Rev. 98 (1998) 2527.
[14] J.M. Lawson, A.M. Oliver, D.F. Rothenfluh, Y.-Z. An, G.A. Ellis, M.G. Ranasinghe, S.I. Khan, A.G. Franz, P.S. Ganapathi, M.J. Shephard, M.N. Paddon-Row, Y. Rubin, J. Org.Chem. 61 (1996) 5032.
[15] P.A. Liddell, S. Kuciauskas, J.P. Sumida, B. Nash, D. Nguyen, A.L. Moore, T.A. Moore, D. Gust, J. Am. Chem. Soc. 119 (1997) 1400.
[16] D.M. Guldi, M. Maggini, G. Scorrano, M. Prato, J. Am. Chem. Soc. 119 (1997) 974.
[17] H. Imahori, Y. Sakata, Eur. J. Org. (1999) 2445.
[18] J. Llacay, J. Veciana, J. Vidal-Gancedo, J.L. Bourdelande, R. González-Moreno, C. Rovira, J. Org. Chem. 63 (1998) 5201.
[19] D.M. Guldi, S. González, N. Martín, A. Antón, J. Garín, J. Orduna, J. Org. Chem. 65 (2000) 1978.
[20] D.M. Guldi, Chem. Commun. (2000) 321.
[21] D.M. Guldi, C. Luo, T. Da Ros, M. Prato, E. Dietel, A. Hirsch, Chem. Commun. (2000) 375.
[22] D.M. Guldi, C. Luo, T. Da Ros, M. Prato, E. Dietel, A. Hirsch, Chem. Commun. (2000) 373.
[23] Q. Lu, D.I. Schuster, S.R. Wilson, J. Org. Chem. 61 (1996) 4764.
[24] J. Cross, H.A. Jiménez-Vázquez, Q. Lu, M. Saunders, D.I. Schuster, S.R. Wilson, H. Zhao, J. Am. Chem. Soc. 118 (1996) 11454.
[25] G. Schick, A. Hirsch, H. Mauser, T. Clark, Chem. Eur. J. 2 (1996) 935.
[26] F. Djojo, A. Herzog, I. Lamparth, F. Hampel, A. Hirsch, Chem. Eur. J. 2 (1996) 1537.
[27] F. Djojo, A. Hirsch, Chem. Eur. J. 4 (1998) 344.
[28] L. Pasimeni, A. Hirsch, I. Lamparth, A. Herzog, M. Maggini, M. Prato, C. Corvaja, G. Scorrano, J. Am. Chem. Soc. 119 (1997) 12896.
[29] M. Taki, S. Sugita, Y. Nakamura, E. Kasashima, E. Yashima, Y. Okamoto, J. Nishimura, J. Am. Chem. Soc. 119 (1997) 926.
[30] K.M. Kadish, X. Gao, E. Van Caemelbecke, T. Suenobu, S. Fukuzumi, J. Am. Chem. Soc. 122 (2000) 563.
[31] A. Bax, M.F. Summers, J. Am. Chem. Soc. 108 (1986) 2073.
[32] P.R. Birkett, A.G. Avent, A.D. Darwish, H.W. Kroto, R. Taylor, D.R.M. Walton, J. Chem. Soc., Chem. Commun. (1993) 1230.
[33] G.A. Burley, P.A. Keller, S.G. Pyne, G.E. Ball, Chem. Commun. (2000) 1717.

ARTICLE B

Títol: Isolation and Characterization of Four Isomers of a C_{60} Bisadduct with a TTF Derivative. Study of their Radical Ions.

Autors: M. Mas-Torrent, R. Rodríguez-Mias, M. Solà, M. A. Molins, M. Pons, J. Vidal-Gancedo, J. Veciana and C. Rovira.

Publicació: *J. Org. Chem*., 67, 566-575.

Any: 2002

Isolation and Characterization of Four Isomers of a C_{60} Bisadduct with a TTF Derivative. Study of Their Radical Ions

M. Mas-Torrent,[†] R. A. Rodríguez-Mias,[‡] M. Solà,[‡] M. A. Molins,[⊥] M. Pons,[§] J. Vidal-Gancedo,[†] J. Veciana,[†] and C. Rovira*[,†]

Institut de Ciència de Materials de Barcelona (CSIC), Campus Universitari de Bellaterra, 08193 Cerdanyola, Spain, Institut de Química Computacional, i Departament de Química, Universitat de Girona, Campus Montilivi, 17071 Girona, Spain, Departament de Química Orgànica, Facultat de Química, Universitat de Barcelona, Martí i Franqués 1, 08028 Barcelona, Spain, and Serveis Cientificotècnics, Lluís Solé i Sabarís, 08028 Barcelona, Spain

cun@icmab.es

Received July 25, 2001

A family of triads composed of C_{60} attached by a rigid spacer to two identical TTF moieties has been synthesized, and some of the isomers have been isolated and characterized by UV-vis spectroscopy, LDI-TOF-MS, and HMBC NMR spectroscopy. AM1 semiempirical calculations of the dipolar moments and the heats of formation of the different isomers have been carried out in order to verify their assignments. Oxidation and reduction of the triads affords the derived radical ion systems, $TTF^{+\bullet}-C_{60}-TTF^{+\bullet}$ and $TTF-C_{60}^{-\bullet}-TTF$, which were studied by EPR spectroscopy. Spin density distributions of these radical cations and radical anions show that the unpaired electron is located mainly on the TTF and fullerene moieties, respectively. However, while the EPR signals obtained from the radical cations are very similar for all the isomers, the structured signals observed for the radical anions arising from the coupling of the unpaired electron with the hydrogen atoms of the methylene bridges in the spacer show that there is a strong influence of the isomerism on the spin distribution. Importantly, the theoretical calculations of the spin density distributions of the radical anions fit well with the experimental EPR results.

Introduction

C_{60} appears to undergo reactions associated with poorly conjugated electron-deficient alkenes. However, a unique feature of C_{60} is that a large number of products may arise from polyaddition since it has 30 reactive [6,6] double bonds. Polyadducts of C_{60} with well-defined three-dimensional structure are of great importance as they possess biological[1a] and material properties.[1b,c] Up to now, several electron donors such as porphyrins, ferrocenes, tetrathiafulvalenes (TTFs), and phthalocyanines have been attached to the fullerene cage,[2−13] and, in a few cases, the final compounds show interesting intramolecular electronic interactions between the C_{60} and the addends. Some of these donor−acceptor dyads form long-lived charge-separated species upon irradiation[9−12] and therefore are interesting systems as molecular building blocks in electrooptical and photovoltaic devices, as well as bistable molecular information storage units.[14]

We have been working with dyads composed of TTF derivatives linked to a C_{60} moiety by a bismethylene bridge, obtained through a Diels−Alder reaction, in which photoexcitation of the fullerene moiety leads to

* Corresponding author. Phone: +(34)-935801853 extn. 245; Fax: +(34)-935805729;.

[†] Institut de Ciència de Materials de Barcelona (CSIC).

[‡] Universitat de Girona.

[§] Universitat de Barcelona.

[⊥] Serveis Cientificotècnics.

(1) (a) Friedman, S. H.; De Camp, D. L.; Sijbesma, R. P.; Srdanov, G.; Wudl, F.; Kenyon, G. L. *J. Am. Chem. Soc.* **1993**, *115*, 6506. (b) Hirsch, A. *Adv. Mater.* **1993**, *5*, 859. (c) Prato, M. *J. Mater. Chem.* **1997**, *7*, 1097.

(2) (a) Rubin, Y.; Khan, S.; Freedberg, D. I.; Yeretzian, C. *J. Am. Chem. Soc.* **1993**, *115*, 344. (b) Rubin, Y.; Khan, S. I.; Oliver, A. M.; Paddon-Row, M. N. *J. Am. Chem. Soc.* **1993**, *115*, 4919. (c) Mullen, K.; Belik, P.; Gügel, A.; Spickermann, J. *Angew. Chem., Int. Ed. Engl.* **1993**, *32*, 78. (d) Liddell, P.; Mcpherson, A. N.; Sumida, J.; Demanche, L.; Moore, A. L.; Moore, T. A.; Gust, D. *Photochem. Photobiol.* **1994**, *595*, 365. (e) Linssen, T. G.; Dürr, K.; Hannack, M.; Hirsch, A. *J. Chem. Soc., Chem. Commun.* **1995**, 103.

(3) Matsubara, Y.; Tada, H.; Nagase, S.; Yoshida, Z. *J. Org. Chem.* **1995**, *60*, 5372.

(4) Isaacs, L.; Haldimann, T. G.; Diederich, F. *Angew. Chem. Int. Ed. Engl.* **1994**, *33*, 2339.

(5) Boulle, C.; Rabreau, J.-M.; Hudhomme, P.; Cariou, M.; Jubault, M.; Gorgues, A.; Orduna, J.; Garín, J. *Tetrahedron Lett.* **1997**, *38*, 3909.

(6) Imahori, H.; Sakata, Y. *Adv. Mater.* **1997**, *9*, 537.

(7) Martín, N.; Sánchez, L.; Illescas, B.; Pérez, I. *Chem. Rev.* **1998**, *98*, 2527.

(8) (a) Lawson, J. M.; Oliver, A. M.; Rothenfluh, D. F.; An, Y.-Z.; Ellis, G. A.; Ranasinghe, M. G.; Khan, S. I.; Franz, A. G.; Ganapathi, P. S.; Shephard, M. J.; Paddon-Row, M. N.; Rubin, Y. *J. Org. Chem.* **1996**, *61*, 5032. (b) Liddell, P. A.; Kuciauskas, S.; Sumida, J. P.; Nash, B.; Nguyen, D.; Moore, A. L.; Moore, T. A.; Gust, D. *J. Am. Chem. Soc.* **1997**, *119*, 1400. (c) Guldi, D. M.; Maggini, M.; Scorrano, G.; Prato, M. *J. Am. Chem. Soc.* **1997**, *119*, 974. (d) Boulle, C.; Rabreau, S.-M.; Hudhomme, P.; Cariou, M.; Jubault, M.; Gorgues, A.; Orduna, J.; Garin, J. *Tetrahedron Lett.* **1997**, *38*, 3909.

(9) (a) Imahori, H.; Sakata, Y. *Eur. J. Org. Chem.* **1999**, 2445. (b) Fujitsuka, M.; Ito, O.; Imahori, H.; Yamada, K.; Yamada, H.; Sakata, Y. *Chem. Lett.* **1999**, 721.

(10) Llacay, J.; Veciana, J.; Vidal-Gancedo, J.; Bourdelande, J. L.; González-Moreno, R.; Rovira, C. *J. Org. Chem.* **1998**, *63*, 5201.

(11) (a) Guldi, D. M.; González, S.; Martín, N.; Antón, A.; Garín, J.; Orduna, J. *J. Org. Chem.* **2000**, *65*, 1978. (b) Martín, N.; Sánchez, L.; Hernanz, M. A.; Guldi, D. M. *J. Phys. Chem.* **2000**, *104*, 4648.

(12) (a) Guldi, D. *Chem. Commun.* **2000**, 321. (b) Guldi, D. M.; Luo, C.; Da Ros, T.; Prato, M.; Dietel, E.; Hirsch, A. *Chem. Commun.* **2000**, 375. *Ibid.* 373.

(13) (a) Prato, M.; Maggini, M.; Giacometti, C.; Scorrano, G.; Sandonà, G.; Farina, G. *Tetrahedron* **1996**, *52*, 5221. (b) Martín, N.; Sánchez, L.; Seoane, C.; Andreu, R.; Garín, J.; Orduna, J. *Tetrahedron Lett.* **1996**, *37*, 5979. (c) Martín, N.; Pérez, I.; Sánchez, L.; Seoane, C. *J. Org. Chem.* **1997**, *62*, 5690.

(14) (a) Sariciftci, N. S.; Smilowitz, L.; Heeger, A. J.; Wudl, F. *Science* **1992**, *258*, 1474. (b) Yu, G.; Pakbaz, K.; Heeger, A. J. *Appl. Phys. Lett.* **1994**, *64*, 3422.

10.1021/jo010748f CCC: $22.00
Published on Web 12/22/2001

Chart 1

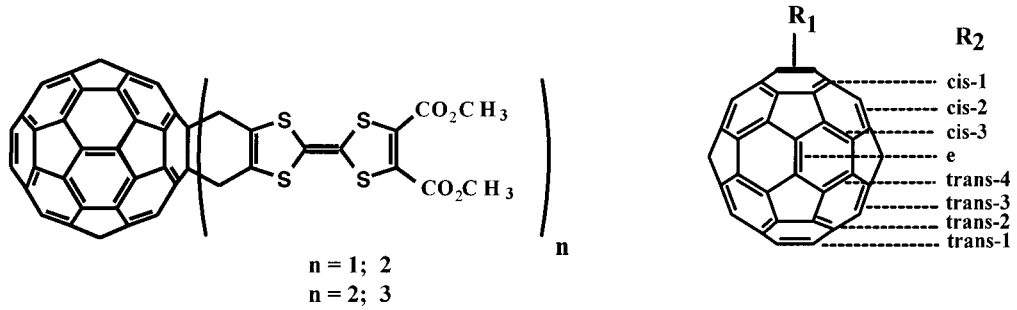

transient charge-separated open-shell species with very long lifetimes.[10] In these dyads, the C_{60} electron acceptor and the TTF electron donor are directly united by two rigid σ bonds which provide not only short separation but also a rigid bridge between them and therefore a well-defined relative distance and orientation.

The synthesis of triads ($C_{60}R_2$) is of great interest for studying the influence of the isomerism on the physical properties,[15−27] despite the fact that there are not many precedents due to the laborious task of isolation and characterization of the isomers. As crystals of these compounds suitable for X-ray structure determination are usually difficult to obtain,[28,29] the assignment of the correct structure for all the isomers has become an important aim, and several groups have been seeking a systematic method to characterize them. Different criteria, such as polarity and UV-vis and NMR spectroscopic data, have been commonly used to imply their nature. Wilson and Schuster have also attempted to correlate the structure of bisadducts exploiting the ^{3}He chemical shifts in the NMR spectra of ^{3}He@C_{60} fullerene derivatives,[16] and Pasimeni et al. suggested a new method based on an EPR study of the excited triplet state of the bisadducts.[21] It has been also shown previously that INADEQUATE NMR[30] and HMBC NMR[31] are useful tools in their characterization.

Herein, we report the study of a family of triads formed by two identical TTF moieties attached to the fullerene cage **3** (Chart 1). The electrochemically generated radical ion systems, $TTF^{+\bullet}-C_{60}-TTF^{+\bullet}$ and $TTF-C_{60}^{-\bullet}-TTF$, show interesting features regarding the influence of the isomerism on the spin distribution in the molecules. Moreover, an extended theoretical study by means of semiempirical and density functional methods has also been carried out in order to interpret the experimental observations, in particular the order of elution in chromatography and the EPR spectra.

Results and Discussion

Synthesis and Characterization of the Bisadducts. A Diels−Alder reaction was used for the synthesis of the triad **3**, which was achieved either by direct bisaddition of the diene, generated upon elimination of SO_2 from bis(methoxycarbonyl)-3-sulfolene-tetrathiafulvalene **1**, to the fullerene[10] or by a second cycloaddition to the monoadduct **2** (Scheme 1). In the former reaction, a mixture of nonreacted C_{60}, monoadduct **2**, and bisadducts **3** was obtained, which were separated by column chromatography. The isolated monoadduct **2** was used as a reagent for the second synthetic pathway, in which the mixture of isomers of **3** was also separated from the nonreacted monoadduct **2** and polyadducts by column chromatography. Depending on the relative position of the addends in the fullerene cage, eight regioisomers can be formed (Chart 1), which were detected by analytical HPLC on silica gel as stationary phase and 0.3% AcOEt in CH_2Cl_2 as mobile phase (Figure 1). Further separation of the very insoluble mixture of regioisomers with a semipreparative silica column enabled the isolation of a few milligrams of four of the isomers, **3a**, **3c**, **3e**, and **3f**. The laser desorption−ionization time-of-flight (LDI-TOF) mass spectra of all of them as well as of those corresponding to the other chromatographic peaks show the molecular peak at *m*/*z* 1412, which confirms that they are isomers of **3**. However, it is worth pointing out that the fraction corresponding to the last peak in the chromatogram **3h** should be attributed to a trisadduct, as a low intensity peak at *m*/*z* 1759 was observed. We want to highlight that the difficult task of isomer separation

(15) Lu, Q.; Schuster; D. I.; Wilson, S. R. *J. Org. Chem.* **1996**, *61*, 4764−4768.
(16) Cross, J.; Jiménez-Vázquez, H. A.; Lu, Q.; Saunders, M.; Schuster, D. I.; Wilson, S. R.; Zhao, H. *J. Am. Chem. Soc.* **1996**, *118*, 11454.
(17) Schick, G.; Hirsch, A.; Mauser, H.; Clark, T. *Chem. Eur. J.* **1996**, *2*, 935.
(18) Hirsch, A.; Lamparth, I.; Karfunkel, H. R. *Angew. Chem., Int. Ed. Engl.* **1994**, *33*, 437.
(19) Djojo, F.; Herzog, A.; Lamparth, I.; Hampel, F.; Hirsch, A. *Chem. Eur. J.* **1996**, *2*, 1537.
(20) Djojo, F.; Hirsch, A. *Chem. Eur. J.* **1998**, *4*, 344.
(21) Pasimeni, L.; Hirsch, A.; Lamparth, I.; Herzog, A.; Maggini, M.; Prato, M.; Corvaja, C.; Scorrano, G. *J. Am. Chem. Soc.* **1997**, *119*, 12896.
(22) (a) Taki, M.; Sugita, S.; Nakamura, Y.; Kasashima, E.; Yashima, E.; Okamoto, Y.; Nishimura, J. *J. Am. Chem. Soc.* **1997**, *119*, 926. (b) Nakamura, Y.; Asami, A.; Inokuma, S.; Ogawa, T.; Kikuyama, M.; Nishimura, J. *Tetrahedron Lett.* **2000**, *41*, 2193. (c) Nakamura, Y.; O-kawa, K.; Matsumoto, M.; Nishimura, J. *Tetrahedron* **2000**, *56*, 5429. (d) Nakamura, Y.; Tacano, N.; Nishimura, T.; Yashima, E.; Sato, M.; Kudo, T.; Nishimura, J. *Org. Lett.* **2001**, *3*, 1193. (e) Ishi-I, T.; Shinkai, S. *Tetrahedron* **1999**, *55*, 12515.
(23) Beulen, M. W. J.; Rivera, J. A.; Herranz, M. A.; Illescas, B.; Martín, N.; Echegoyen, L. *J. Org. Chem.* **2001**, *66*, 4393.
(24) Diedrich, F.; Kessinger, R. *Acc. Chem. Res.* **1999**, *32*, 537.
(25) (a) Nakamura, Y.; Taki, M.; Tobita, S.; Shizuka, H.; Yokoi, H.; Ishiguro, K.; Sawaki, Y.; Nishimura, J. *J. Chem. Soc., Perkin Trans. 2* **1999**, 127. (b) Sun, Y.-P.; Guduru, R.; Lawson, G. E.; Mullins, J. E.; Guo, Z.; Quinlan, J.; Bunker, C. E.; Gord, J. R. *J. Phys. Chem. B* **2000**, *104*, 4625.
(26) (a) Da Ros, T.; Prato, M.; Lucchini, V. *J. Org. Chem.* **2000**, *65*, 4289. (b) Kordatos, K.; Bosi, S.; Da Ros, T.; Zambon, A.; Lucchini, V.; Prato, M. *J. Org. Chem.* **2001**, *66*, 2802.
(27) Kreher, D.; Liu, S.-G.; Cariou, M.; Hudhomme, P.; Gorgues, A.; Mas, M.; Veciana, J.; Rovira, C. *Tetrahedron Lett.* **2001**, *42*, 3447.
(28) Woods, C. R.; Bourgeois, J.-P.; Seiler, P.; Diedrich, F. *Angew. Chem., Int. Ed.* **2000**, *39*, 3813.
(29) Kadish, K. M.; Gao, X.; Van Caemelbecke, E.; Suenobu, T.; Fukuzumi, S. *J. Am. Chem. Soc.* **2000**, *122*, 563.
(30) Burley, G. A.; Keller, P. A.; Pyne, S. G.; Ball, G. E. *Chem. Commun.* **2000**, 1717.
(31) Mas-Torrent, M.; Pons, M.; Molins, M. A.; Veciana, J.; Rovira, C. *Synth. Met.* **2001**, *123*, 523.

Scheme 1

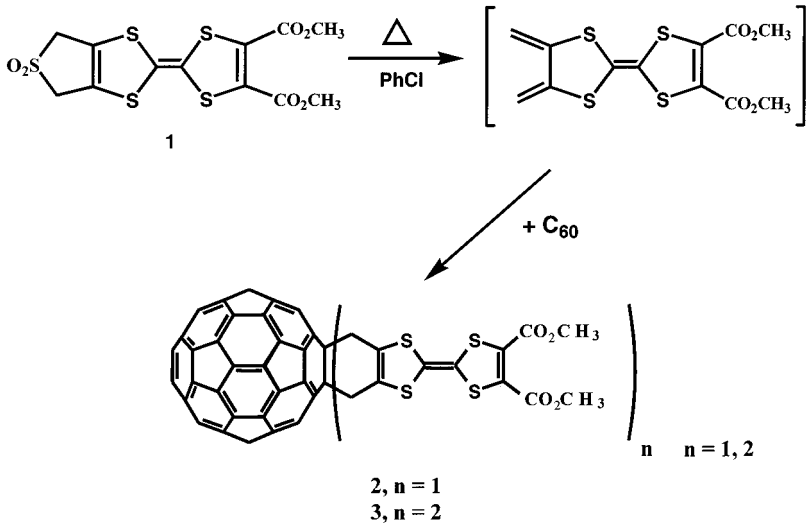

1

2, n = 1
3, n = 2

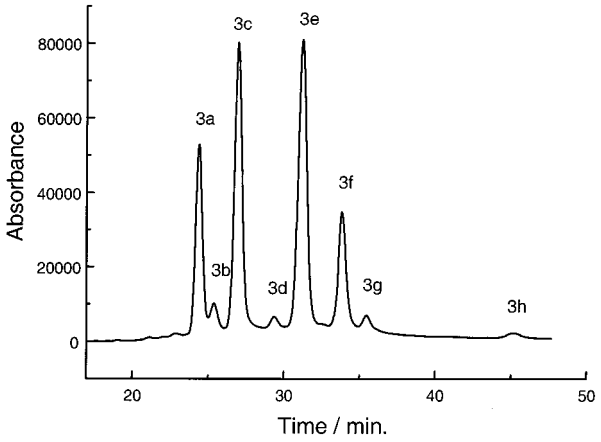

Figure 1. HPLC chromatogram of the mixture of isomeric bisadducts of **1**. Conditions: 25 × 0.46 cm Spherisorf Silica column, 0.3% AcOEt in CH_2Cl_2 (1 mL/min), UV-vis detection at 290 nm.

was confounded by the formation of aggregates in the solvents required to have a good separation (CH_2Cl_2/AcOEt). It is well-known that C_{60} forms aggregates through intermolecular $\pi-\pi$ interactions,[32] resulting in broad peaks in the HPLC chromatogram and making it difficult to attain pure isomers. This problem was partially solved by treating the sample, prior to the injection in the HPLC column, with aromatic solvents such as toluene or chlorobenzene, as $\pi-\pi$ interactions of solvent molecules with the C_{60} compounds destroys the aggregates. However, the complete disaggregation of the sample is not possible, and therefore the isolation of the last eluted isomers in a pure state is extremely challenging, to the point that the last HPLC-eluted isomers are often contaminated with the first ones. The structure of the isomers corresponding to the different fractions were assigned by UV-vis spectroscopy, HMBC spectroscopy, and using polarity arguments.

At first glance, the order of elution expected in the HPLC (silica gel) for the regioisomers of **3** can be based on the increasing polarity with decreasing distance between addends (*trans-1*, *trans-2*, *trans-3*, *trans-4*, *equatorial*, *cis-3*, *cis-2*, and *cis-1*). Nevertheless, experimental results for different compounds do not always coincide with predictions based on this argument. While Bingel bisadducts and spiromethano fullerenes follow the theoretical elution order,[17−20] in the Diels−Alder and benzyne bisadducts studied by Nishimura et al. the order of the *cis* isomers changes, the elution order being *trans-1*, *trans-2*, *trans-3*, *trans-4*, *e*, *cis-1*, *cis-2*, and *cis-3*.[22c,d] In addition, fulleropyrrolidine bisadducts show the elution order: *trans-1*, *trans-2*, *trans-3*, *cis-1*, *trans-4*, *e*, *cis-2* and *cis-3*.[26b] Also, depending on the steric requirements of the addends, some of the isomers can be less favored. For these reasons, before attempting the assignment of regioisomers of **3**, we performed semiempirical calculations of their dipolar moments as well as their heats of formation.

Since it was found that heat of formation of *cis-2* and *cis-1* isomers in their most stable conformations was higher in energy by about 8 and 15 kcal mol^{-1}, respectively, than those required for the formation of the rest of the isomers (*trans-1*, *trans-2*, *trans-3*, *trans-4*, *e*, and *cis-3*), we did not include them in the following calculations. For each isomer, four conformations arising from to the boat-to-boat inversion are possible. Previous works[2a,33] have shown that the energy barrier for the boat-to-boat inversion in C_{60} is relatively low (about 15 kcal mol^{-1}), and therefore one can expect that at room temperature there is a rapid equilibrium taking place between all possible conformers. Furthermore, the rotation of the methoxycarbonyl groups leads to additional conformers. Calculations indicate that the most stable conformations are those having the two methoxycarbonyl groups in one TTF unit located perpendicularly (see Figure 2). One group remains planar with respect to the TTF unit, taking benefit of the additional conjugation, while the other is placed perpendicularly due to steric hindrance. Taking into account this fact, four possible conformers due to rotation of the methoxycarbonyl groups for each TTF unit are possible. Overall, we have considered six different regioisomers and for each of them we

(32) (a) Ahn, J. S.; Suzuki, K.; Iwasa, Y.; Otsuka, N.; Mitani, T. *J. Luminisc.* **1998**, *76−7*, 201. (b) Nath, S.; Pal, H.; Palit, D. K.; Sapre, A. V.; Mittal, J. P. *J. Phys. Chem. B* **1998**, *102*, 10158. (c) Rudalevige, T.; Francis, A. H.; Zand, R. *J. Phys. Chem. A* **1998**, *102*, 9797. (d) Thomas, K. G.; Biju, V.; Guldi, D. M.; Kamat, P. V.; George, M. V. *J. Phys. Chem. B* **1999**, *103*, 8864.

(33) Shepard, M. J.; Paddon-Row, M. N. *Aust. J. Chem.* **1996**, *49*, 395.

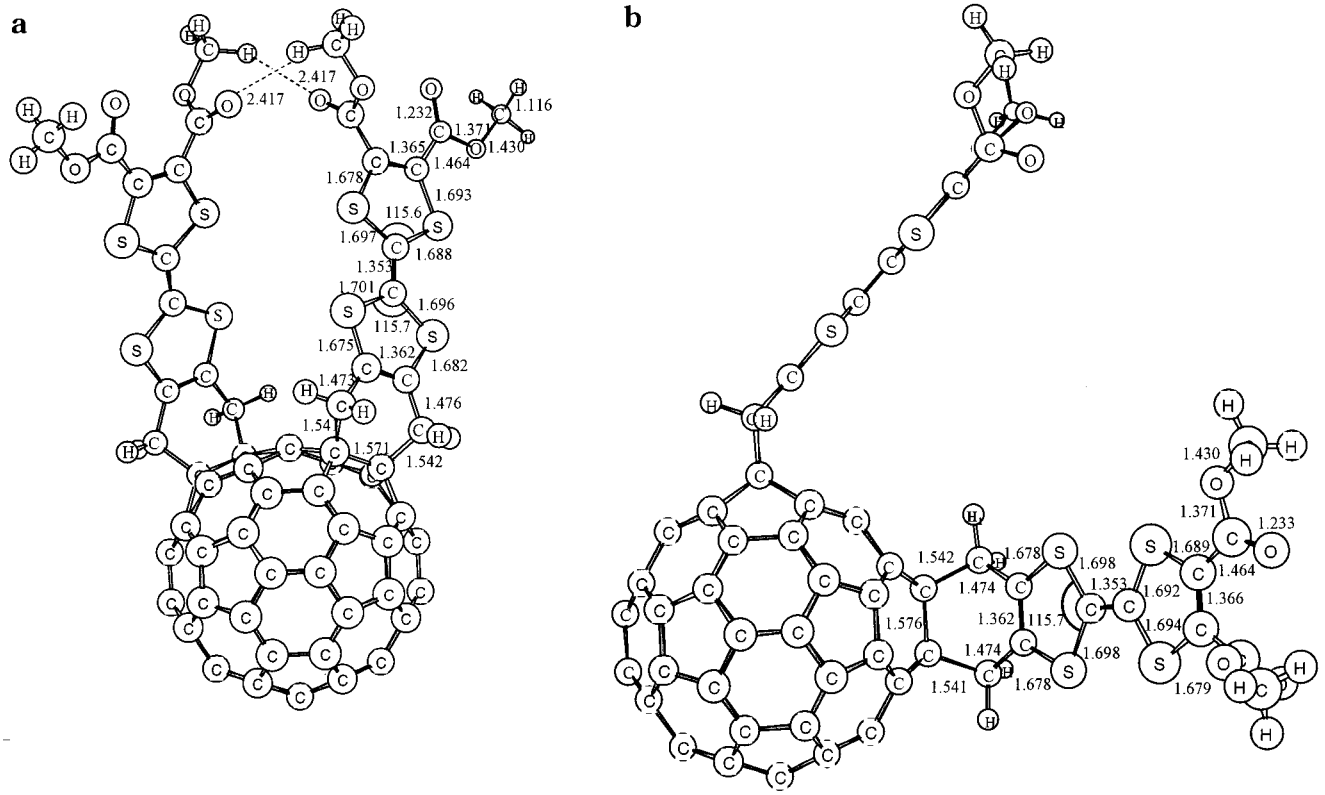

Figure 2. AM1-optimized geometry of the gas-phase most stable boat-to-boat conformer for (a) the *cis-3* regioisomer; (b) the *equatorial* regioisomer.

have considered 64 possible conformers. The only exception is the boat-to-boat conformer of the *cis-3* regioisomer depicted in Figure 2a. In this case, to avoid steric repulsion because of the proximity of the two TTF units, the two nearest methoxycarbonyl groups are located perpendicularly to the TTF units, with their carbonyl groups facing one each other. Therefore, only one possible conformer out of 16 is possible in this particular boat-to-boat conformer. As a whole, a total of 369 conformers have been calculated, although, for symmetry reasons, some of them are equivalent.

Surprisingly, it was found that the dipole moment of the isomer depends greatly on its conformation. In particular, the position of the methoxycarbonyl groups has an enormous influence on the dipole moment. For instance, the value of the dipole moment for the *trans-1* regioisomer varies from 0.00 to 6.01 D, while that of the *trans-2* isomer from 0.33 to 6.98 D. Indeed, depending on the conformation, the *trans-1* isomer can be even more polar than the *cis-3* isomer. As a consequence, for this particular derivative **3**, the use of the expected polarity (based on the relative position of the addends) to assign the order of elution without further checking is questionable. For this reason we have theoretically assigned a dipole moment to each regioisomer by computing the dipole moment of all conformers considered (for further information see the Computational Details). Table 1 gathers the values of the dipole moments obtained in this way. It is seen that the polarity found theoretically is in accordance to what was expected on the basis of relative position of the two TTF units in the fullerene core, the polarity decreasing in the order *cis*-3, *e*, *trans-4*, *trans-3*, *trans-2*, and *trans-1* regioisomers.

Experimentally, the synthesis of isomer **3** takes place in toluene solution at 120 °C. Given the low dielectric constant of toluene, we have used the calculated Gibbs energy in gas phase at 393 K to calculate the theoretical relative abundances of the regioisomers, considering now a Maxwell−Boltzmann distribution of all possible conformers of the *cis*-3, *e*, *trans-4*, *trans-3*, *trans-2*, and *trans-1* regioisomers. The results of theoretical relative abundances together with the experimental product distribution obtained from the different HPLC chromatogram peak areas are listed in Table 1. The experimental results differ significantly from the theoretical ones, especially in the case of the *trans-4* regioisomer, indicating that the bisadduct formation probably takes place under kinetic control. A similar conclusion was also reached by Hirsch et al.[34] in the study of multiple nucleophilic cyclopropanations to the fullerene core.

It is also worth pointing out that, for each isomer, the stability of all possible conformations are quite similar, the differences among conformations of the same regio-

Table 1. Assignment of the Chromatographic Peaks Resulting from the Separation of the Isomers of 3

peak	retention time (min)	assignment	μ calcd (D)[a]	% chromatogram peak area	% theoret abundance[b]
3a	24.40	*trans-2*	3.39	16.1	13.1
3b	25.39	*trans-1*	3.13	3.6	1.7
3c	26.99	*trans-3*	3.45	28.8	20.6
3d	29.36	*trans-4*	3.48	2.8	27.8
3e	31.24	*equatorial*	3.57	32.0	36.1
3f	33.85	*cis-3*	3.85	12.9	0.6
3g	35.50	*cis-2*	–	3.0	–
3h	45.20	*trisadduct*	–	0.8	–

[a] Dipole moment in Debeyes. [b] Product distribution at 393 K calculated by AM1 method.

(34) Hirsch, A.; Lamparth, I.; Grösser, T. *J. Am. Chem. Soc.* **1994**, *116*, 9385.

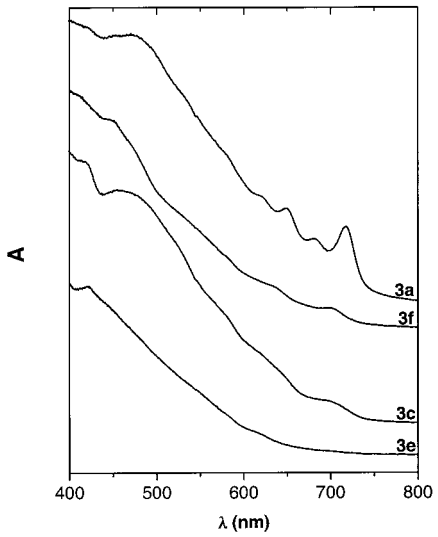

Figure 3. Visible absorption spectra of regioisomers **3a** (*trans-2*), **3c** (*trans-3*), **3e** (*equatorial*), and **3f** (*cis-3*) in CH_2Cl_2.

isomer being always smaller than 0.4 kcal mol^{-1}, with the exception of isomer *cis-3*, in which the conformation depicted in Figure 2a is more stable than the rest by about 1 kcal mol^{-1}. This gain of stability is attributed to the formation of two C−H···O hydrogen bonds between the carboxymethyl groups of the two addends. However, in solution this conformation is particularly destabilized by the proximity of the two TTF units which leads to a decrease of the total solvent accessible surface by about 100 $Å^2$, which in turn is responsible for the reduction of the solvation free energy of this conformer by ca. 3 kcal mol^{-1}.

On the other hand, the experimental results available at present indicate that the electronic properties of a given bisadduct depend principally on the addition pattern rather than the nature of the addend. Especially, the characteristic features in the region between 400 and 800 nm can be used as a fingerprint for the identification of a given regioisomer.[17,18] Hence, comparing the electronic spectra obtained for **3a**, **3c**, **3e**, and **3f** (Figure 3) with the ones found in the literature[15,19,22,23,26b] and taking into account the former dipole moment calculations that permit the estimation of the order of elution, it is possible to make a reasonable assignment of isomers **3a**, **3c**, **3e**, and **3f** to isomers *trans-2*, *trans-3*, *e*, and *cis-3* respectively (Table 1). Thus, the position, intensity and the width of the bands in the Visible spectrum of isomers **3a** and **3c** are almost identical to those observed for the *trans-2* and *trans-3* isomers in the bisadducts of *o*-quinodimethane,[22b] fulleropyrrodiline,[26b] and benzyne[22d] derivatives and quite similar to those reported for other bisadducts.[19,23] Isomer **3e** shows the same spectrum as those of the *equatorial* isomers of quinodimethane,[22a,c,e] and fulleropyrrodiline[26b] derivatives. The visible spectrum of isomer **3f** has the same characteristic features as those of *cis-3* isomers of of *o*-quinodimethane,[22a,b] fulleropyrrodiline,[26] and benzyne[22d] derivatives as well as anisyl and methanofullerenes.[19,23] These features are quite different from those shown by the corresponding *cis-2* isomers especially in the 600−750 nm region, thus permitting the assignment of *cis-3* isomer to **3f**.

It is worth noting that this assignment fits with the one expected according to the order of elution with the exception of the *trans-2* isomer, which elutes before *trans-1*. However, similar changes in the elution order have also been observed in other C_{60}-bisadducts and always with those isomers that have much less abundance than the corresponding neighbors.[19,26b]

The complete characterization of the regioisomers of **3** should be performed by NMR, but good ^1H and ^{13}C NMR spectra were not plausible on account of the very low solubility of these compounds. Nevertheless, thanks to the use of the HMBC technique, the NMR characterization of two of them was possible, and it is in good agreement with the previous assignment of the isomers.[35] In particular, isomers **3a** (*trans-2*) and **3e** (*equatorial*) have been studied by HMBC, and the spectra obtained are in accord with their symmetry.[31] The assignment of the chemical shifts are summarized in Table 2. The unexpected low frequency of one of the protons of a methylenic group of bisadduct **3e** (H_1) can be attributed to ring current effects arising from the π system of the other TTF addend, that according to the theoretical structure is situated in a molecular plane almost perpendicular to the H_1 proton (Figure 2b). Moreover, the C_{A2} carbon atom of the same isomer and also one of the adjacent carbon atoms of the isomer **3a** resonate at ca. 160 ppm, more than 6 ppm higher than the other adjacent carbon atoms. As a matter of fact, the relative disposition of the anomalous C_A with respect to the anchoring bond of the TTF addend, along a pathway defined by two connected 5-radialene units, is the same for both *trans-2* (**3a**) and *equatorial* (**3e**) isomers. If this observation about some adjacent carbon atoms appearing at an unexpected chemical shift only in some of the isomers can be generalized, it may provide an additional simple tool for the characterization of C_{60} bisadducts. In support of this hypothesis, we note thet the C_A of *trans-2* and *equatorial* isomers of bisadducts of fulleropyrrolidine derivatives resonate also around 160 ppm.[26b]

Study of the Radical Ion Derivatives. The presence on the same molecule of electron donor and acceptor moieties makes possible the generation of their radical-cation and radical-anion derivatives by oxidation or reduction, respectively (Scheme 2).[36]

In the study of the radical cations of **3** it is necessary to take into account that since molecule **3** has two TTF addends, it is possible to form the monoradical cations and the biradical cations by oxidation of the isomers of **3**. It is interesting to note that if only one of the TTF addends is oxidized, the resulting cation radical is a mixed valence compound, a very attractive species because it can present intramolecular electron transfer through the fullerenic bridge promoted by an external optical or thermal stimulus. In such a case, the different isomers can even present different rates in this process. To study accurately this process, quantitative spectroelectrochemical experiments should be performed, and, in our case, this has not been possible due to the very small amounts of each pure isolated isomer.

The radical cations of bisadducts **3a** (*trans-2*), **3c** (*trans-3*), **3e** (*e*), and **3f** (*cis-3*) were generated by electrochemical oxidation and monitored by EPR and UV-

(35) The other isomers were not obtained pure in enough quantity for determination of a good ^1H NMR spectra.

(36) In the cyclic voltammetry in CH_2Cl_2 of the mixture of isomers of **3**, two reversible oxidation processes at 0.67 and 1.14 V (versus Ag/AgCl) corresponding to the TTF's and up to three quasi-reversible reduction processes due to the C_{60} at −0.66 V, −1.02 V, and −1.45 V (versus Ag/AgCl) are observed (see ref 10).

Table 2. NMR Data of Triads 3a (*trans-2*) and 3e (*equatorial*)

	^{1}H chemical shifts (ppm)				^{13}C chemical shifts (ppm)						
	TTF methylenic protons				bridge carbons[a]			adjacent carbons[b]			
isomer	H1	H2	H3	H4	B1	B2	B3	A1	A2	A3	A4
trans-2	4.40−4.60(AB; 15 Hz)		4.35−4.40(AB; 15 Hz)		65.0	64.5	−	153.6	154.4	153.8	160.0
equatorial	3.72(s)	3.98(s)	4.02−4.06(AB; 15 Hz)		65.6	65.2	65.2	154.0	161.0	153.5	154.5

[a] Fullerene Csp^3, bridge carbons between the C_{60} and the TTF. [b] Fullerene Csp^2, carbons adjacent to the bridge ones.

Scheme 2

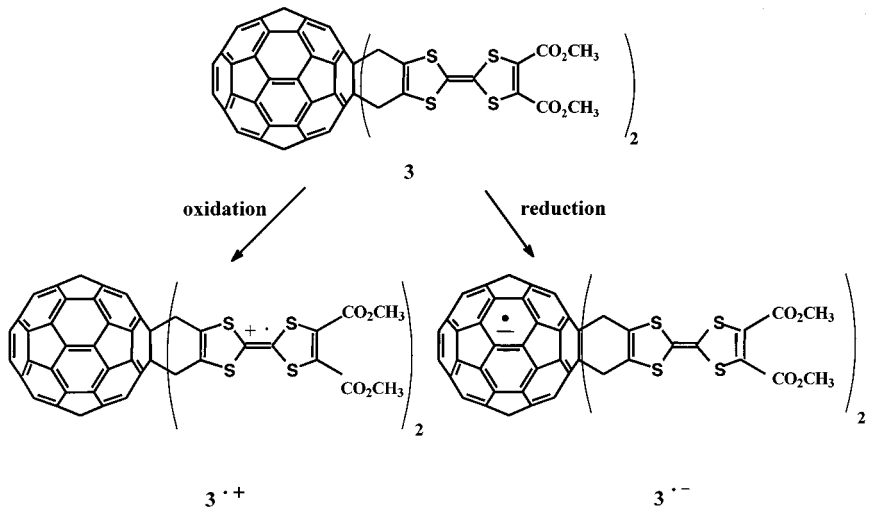

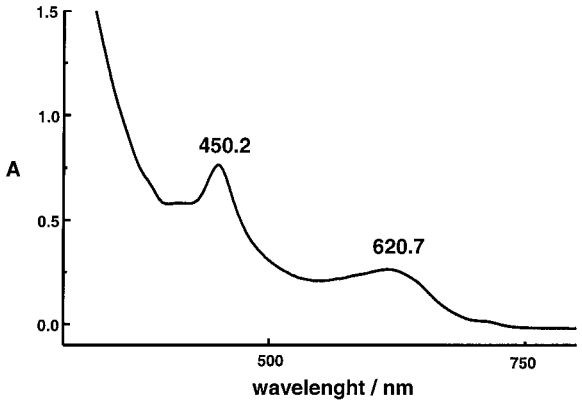

Figure 4. Visible absorption spectrum of the radical cation obtained from **3a** after 10 min of electrochemical oxidation.

vis spectroscopy. These radical cations have appreciable persistency with lifetimes of the order of days. All show new intense bands in the 400−700 nm region of the electronic spectra (Figure 4), not present in the neutral molecules, which are characteristic of radical cations centered on a TTF core.[37] These absorption bands are very similar to those obtained for the radical-cation derived from the monoadduct **2**.[10] In contrast to the spectra of the neutral compounds, all isomers have almost identical spectra dominated by the characteristic TTF cation radical absorption bands, which appear very intense in the same region where weak bands differentiate the neutral compounds. Although oligothiophenes unexpectedly aggregate when attached to fullerenes,[38] the fact that there are no additional bands in the visible spectra of compounds **3** that could be attributed to dimer formation is not so surprising if we take into account the appreciable steric hindrance introduced by the bulky fullerene cage, together with the poor solubilities of these compounds that prevent the preparation of highly concentrated solutions, in which aggregation is favored.

The EPR spectra obtained for the cation radicals of **3a** (*trans-2*), **3c** (*trans-3*), **3e** (*equatorial*) and **3f** (*cis-3*) are almost identical (Table 3). All the studies presented below have been performed "in situ" using a flat electrochemical cell adapted to the EPR spectrometer. During the initial steps of the 'in situ' electrochemical oxidation the central signal obtained (Figure 5a) consists of three lines centered at $g = 2.0077(2)$ with relative intensities 1:2:1 very similar to that obtained from the oxidation of the monoadduct **2**.[10] That triplet signal was attributed to the coupling of the free electron to two axial methylenic protons, since the coupling with the equatorial ones is negligible as they lie on the nodal plane of the SOMO. This differentiation is due to the low rate of the boat-to-boat interconversion on the EPR time scale, a situation also present in the case of other C_{60} cycloadducts.[2a,39] We can assume that in the initial steps of the electrochemical oxidation only the monoradical cation is formed. Thus, the fact that the EPR spectra of all the isomers are almost identical to that obtained from the monoadduct **2**, indicates that at room temperature the unpaired electron is in all cases located only on one of the TTF addends. As the electrochemical oxidation proceeds, the EPR spectra changes, and two additional lines start to appear exactly in the middle of the three main lines (Figure 5b). In all the isomers, the spectra of the biradicals develop toward a quintuplet, but we never obtained the theoretical 1:4:6:4:1 relative intensities of the lines expected for

(37) Torrance, J. B.; Scott, B. A.; Welber, B.; Kaufman, F. B.; Seiden, P. E. *Phys. Rev. B* **1979**, *19*, 730.

(38) Apperloo, J. J.; Langeveld-Voss, B. M. W.; Knol, J.; Hummelen, J. C.; Janssen, R. A. J. *Adv. Mater.* **2000**, *12*, 908.

(39) (a) Tago, T.; Minowa, T.; Okada, Y.; Nishimura, J. *Tetrahedron Lett.* **1993**, *34*, 8461. (b) Zhang, X.; Foote, C. S. *J. Org. Chem.* **1994**, *59*, 5235. (c) Fernández-Paniagua, U. M.; Illescas, B.; Martín, N.; Seoane, C.; Cruz, P.; Hoz, A.; Langa, F. *J. Org. Chem.* **1997**, *62*, 3705.

Table 3. EPR Coupling Constants Corresponding to the Radical Species Derived from 3a (*trans-2*), 3c (*trans-3*), 3e (*e*), and 3f (*cis-3*)

	radical anion a_H/G								radical cation a_H/G	
isomer	H1	H2	H3	H4	H5	H6	H7	H8	monoradical	biradical
trans-2	0.18	0.09	0.18	0.10	0.09	0.18	0.18	0.10	1.93	0.95
trans-3	0.07	0.14	0.26	0.10	0.07	0.09	0.26	0.28	1.91	0.94
equatorial	0.00	0.28	0.09	0.21	0.10	0.09	0.09	0.00	1.94	0.96
cis-3	0.28	0.09	0.06	0.05	0.04	0.00	0.29	0.05	1.94	0.95

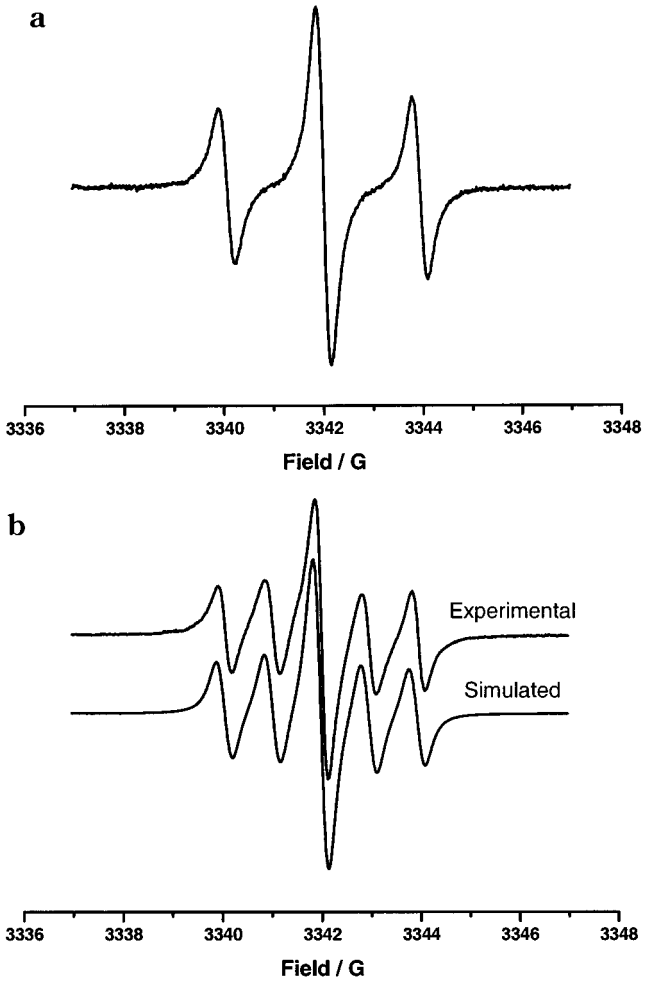

Figure 5. EPR spectra at 293 K in CH_2Cl_2 under isotropic conditions of the radical cation derived from **3c** (*trans-3*) (a) after 5 min of in situ electrochemical oxidation; (b) after 1 h of in situ electrochemical oxidation.

a pure biradical at the fast exchange limit in which the *intramolecular exchange coupling constant* (J^{intra}) between the two electron spins at each TTF addend of the molecule is much bigger than the hyperfine coupling constant with the ^1H nuclear spins; i.e., $J^{intra}/g\beta \gg a_H$.[40] Nevertheless, the fact that the line width of the new lines are exactly the same as those of the three already existing lines seems to rule out the possibility of being in the situation in which J^{intra} has an order of magnitude similar to that of the coupling constant a_H.[41] It seems, therefore, that the spectra obtained correspond to the coexistence of monoradical and biradical species in the solution. Thus, the spectra registered at different oxidation times can be perfectly simulated by the sum, in different proportions, of the spectrum corresponding to the monoradical and that corresponding to the biradical at the fast exchange limit. In Figure 5b, the experimental and simulated EPR spectrum obtained upon oxidation of **3** (isomer *trans-3*) for 1 h is shown; in this case the proportion monoradical:biradical is 1:2. As expected, the coupling constants observed in the biradicals are half those observed for monoradicals (Table 3). On lowering the temperature, we did not observe the $\Delta m_s = 2$ transition of triplet states in any of the biradicals generated. This fact is not surprising since the concentration of the biradical species is always very low, and the distance between the two centers with spin density is long.[42]

Radical anions of isomers **3a** (*trans-2*), **3c** (*trans-3*), **3e** (*e*), and **3f** (*cis-3*) were obtained by electrochemical reduction and were characterized by EPR spectroscopy. As already observed for the anion radical species generated from the mixture of the isomers **3**,[10] the spectra of each isomer show a narrower EPR signal than the one of the radical-anion derived from the monoadduct **2**. This situation permits the observation of the hyperfine structure arising from the coupling of the unpaired electron with the hydrogen atoms of the methylenic groups of the bridges. Therefore, for the first time, the coupling of the electrons of a fulleride with the addend's atoms has been experimentally observed. Contrary to the case of the radical cations, the isomerism does influence the type of signals obtained. Interestingly, it was found that the hyperfine structure of the spectra of the derived radical anions from the above-mentioned isomers are strikingly different to each other. As an example, in Figure 6 we show the experimental and simulated spectra for two of the isomers (**3a**; *trans-2* and **3f**; *cis-3*).

The isotropic coupling constants of the methylenic protons have been calculated and compared with the experimental ones obtained by simulation of the experimental EPR spectra. Due to computational limitations, calculations have been done only for the most stable conformer of each regioisomer in the gas phase. The simulations of EPR spectra were carried out using an iterative least-squares fitting procedure based on Monte Carlo Methods and starting from the B3LYP/3-21G//AM1 calculated proton coupling constants.[43] The results of the simulations are presented in Table 3. The calculated values of the coupling constants are remarkably similar to the experimental ones as can be appreciated on Figure 7, in which the relative experimental coupling constant values are plotted against the calculated ones, and the resulting points of the graph are fitted with a line of slope

(40) Salem, L.; Rowland, C. *Angew. Chem., Int. Engl. Ed.* **1972**, *11*, 92.

(41) (a) Glarum, S. H.; Marshall, J. H. *J. Chem. Phys.* **1967**, *47*, 1374. (b) Brière, R.; Dupeyre, R.-M.; Lemaire, H.; Morat, C.; Rassat, A.; Rey, P. *Bull. Soc. Chim. Fr.* **1965**, *11*, 3290. (c) Hernàndez-Gasio, E.; Mas, M.; Molins, E.; Rovira, C.; Veciana, J.; Borrás-Almenar, J. J.; Coronado, E. *Chem. Mater.* **1994**, *6*, 2398.

(42) Eaton, S. S.; More, K. M.; Sawant, B. M.; Eaton, G. R. *J. Am. Chem. Soc.* **1983**, *104*, 523.

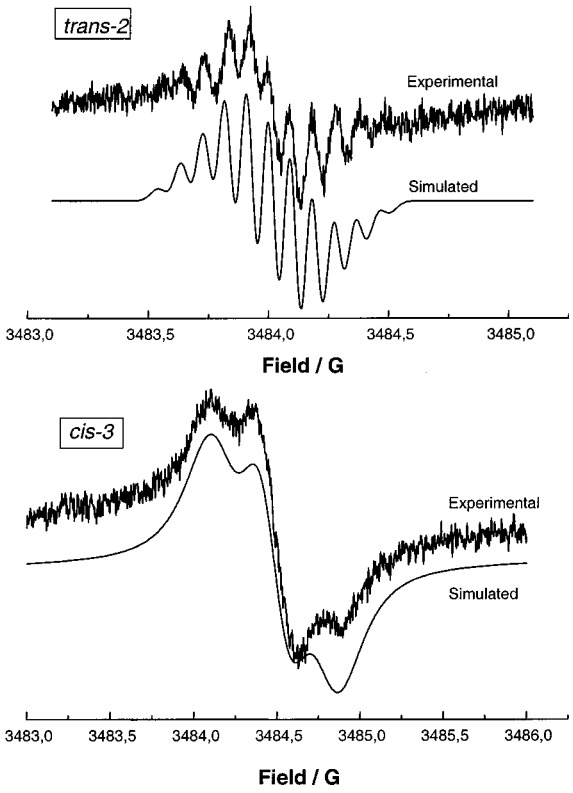

Figure 6. EPR spectra (293 K) in CH_2Cl_2 under isotropic conditions and simulated EPR spectra of the radical anions derived from **3a** (*trans-2*) and **3f** (*cis-3*).

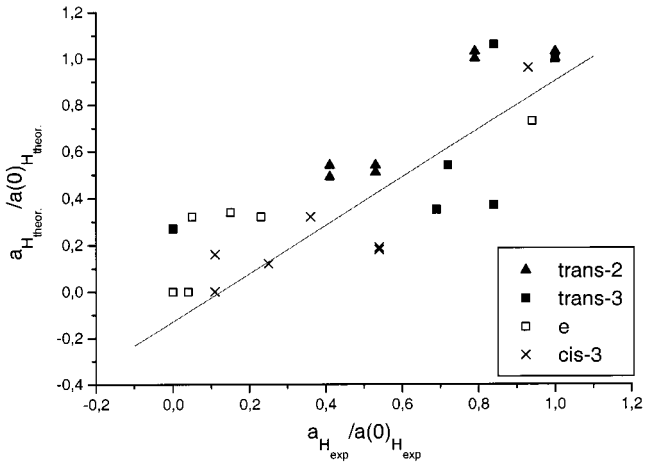

Figure 7. Graphical representation of the relative values of the experimental EPR proton coupling constants versus the calculated ones.

1.03. Therefore, we have shown that the spin density distribution of the anionic species derived from **3** depends strongly on the isomerism, and it has also been shown that the coupling of the unpaired electron with the addend's protons can be predicted by B3LYP/3-21G//AM1 calculations. Thus, the study of the EPR signal of the derived radical anion of C_{60} triads is a potentially extremely useful method for the characterization and assignment of the different isomers.

The experimental values of the hyperfine coupling constants (hfcc's) are excellent proof of the spin density on each nucleus. However, if we want to have an idea of the spin density distribution over the whole molecule, other techniques have to be used. Theoretically, this goal

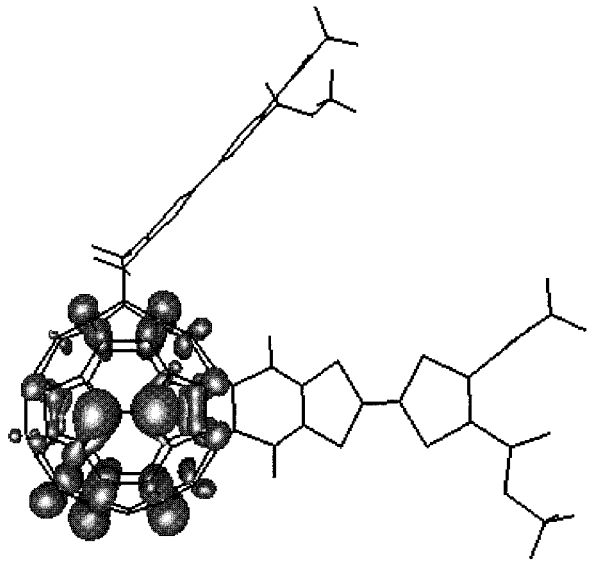

Figure 8. 3D representation of the radical anion spin density of a particular conformer of regioisomer *e* computed at the B3LYP/6-31G**//AM1 level. Isosurface value is 0.001 au.

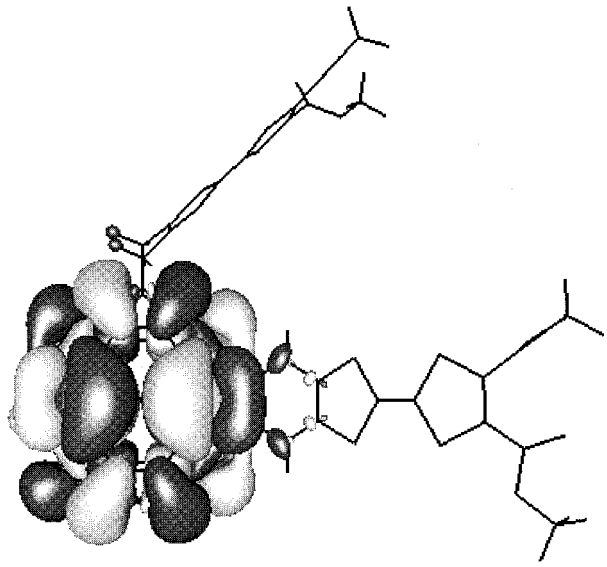

Figure 9. 3D representation of the LUMO of a particular conformer of regioisomer *e* computed at the B3LYP/6-31G**//AM1 level. Isosurfaces values are −0.01 and 0.01 au.

can be achieved through the representation of spin density maps. These maps, which give the value of the spin density at any point of space around the molecule, are calculated by subtracting the electronic density of the α and β electrons. As an example, in Figure 8 the spin density map of a particular conformer of regioisomer *e* computed at the B3LYP/3-21G//AM1 level is presented. Figure 8 shows that the spin density in these species is lower in the region of the fullerene core next to the attached TTF units. Similar results were obtained for the rest of the regioisomers. For the same conformer, Figure 9 depicts the LUMO of the neutral species calculated at the B3LYP/3-21G//AM1 level. It is worth noting that the density of the LUMO orbital of the neutral species differs to some extent from the spin density of the radical anion, although in both cases the amplitude is the highest at the *equatorial* position with respect to the TTF units.

Conclusions

In conclusion, a family of $C_{60}(TTF)_2$ triads has been synthesized and some of the isomers isolated and characterized. In the EPR spectra, it has been seen that there are no differences in the signals obtained for the derived radical cations formed by oxidation of the donor addends. However, by reducing the fullerene cage to obtain the corresponding radical anions, the hyperfine structure of the EPR signal obtained for each isomer shows notable differences. The distinct spin density distribution of the isomers has been studied by density functional calculations and fits with the experimental results. The methodology demonstrated by this study could not only be useful for the characterization of C_{60} triads but also for designing triads with donor addends where charge transfers mediated by the C_{60} can take place.

Experimental Section

Computational Details. Full geometry optimizations without symmetry constraints were carried out with the AM1 semiempirical method[44] as implemented in AMPAC 6.55,[45] a quantum chemistry program from Semichem, Inc. Previous studies have shown that the AM1 method provides reliable results for the geometries and energetics of C_{60},[46] C_{70},[47] and Diels−Alder adducts. AM1 calculations were performed using the restricted formalism. The free energies of formation in gas phase for the different isomers and conformers were calculated from the addition of entropy corrections to the enthalpies of formation. The influence of solvation on the stability of the different species was included by means of self-consistent reaction field methods (SCRF). In particular, SCRF calculations to determine free energies of solvation were performed using the MST model,[48−50] also known as the polarizable continuum model. To simulate the solvent used in HPLC experiments (0.3% of ethyl acetate in methylene chloride) we used the parametrization of the MST/SCRF continuum model corresponding to a chloroform solution.[48,49] The reasons for this choice are that the methylene chloride solvent has not been parametrized yet at the semiempirical AM1 level, and that chloroform and methylene chloride have a similar dielectric constant. Free energies of solvation in chloroform were computed with the AM1 method with a modified version of the MOPAC computer program.[51]

The averaged dipole moment of each regioisomer was obtained by considering a Maxwell−Boltzmann distribution of its conformers and using their Gibbs computed energies at 298 K in solution, that is:

$$\langle \mu_k \rangle = \sum_{i=1}^{n_k} p_i \mu_i \text{ with } p_i = \frac{g_i \exp\left(-\frac{\Delta G_i^o}{RT}\right)}{\sum_{i=1}^{n_k} g_i \exp\left(-\frac{\Delta G_i^o}{RT}\right)}, \qquad (1)$$

where n_k is the total number of conformers of regiosiomer k, and g_i, μ_i, and ΔG_i^o are the degeneration, the dipole moment, and the sum of the formation and solvation Gibbs energies, respectively, of conformer i belonging to regiosiomer k.

For selected systems we have calculated the isotropic hyperfine coupling constants (hfcc) of the methylenic hydrogen atoms of the cyclohexene bridges between the C_{60} and the TTF addend from the electron spin densities at the hydrogen atom using the following equation,

$$a_H = \frac{8\pi}{3} \frac{g_e}{g_o} \gamma_H \beta_H \rho_s(\mathbf{r}_H) \qquad (2)$$

where g_e/g_o is the ratio of the isotropic g value for the radical to that of the free electron, γ_H and β_H are the gyromagnetic nuclear ratio and the nuclear magneton, respectively, for the hydrogen atom, and $\rho_s(\mathbf{r}_H)$ is the spin density on the nucleus of the hydrogen atom considered. The approach we use to evaluate these quantities is the density functional theory in the unrestricted Kohn−Sham (UKS) version.[52] In particular, hfcc's were calculated using the B3LYP[53] density functional with the 3-21G basis set[54] and employing the AM1-optimized geometries of the radical anions (B3LYP/3-21G//AM1). For all radical anions, the S^2-value (where S represents the electronic spin) over the reference Slater determinant of self-consistently converged Kohn−Sham orbitals is very close to the theoretical value for a doublet state (0.75), being always smaller than 0.7552. The isotropic hyperfine coupling constants of free radicals are one of the most challenging one-electron properties for ab initio quantum mechanical methods. Good results are generally found using the B3LYP density functional and basis sets which describe well the core region of the electron density.[55] One can expect that the B3LYP/3-21G//AM1 method will provide at least qualitatively correct hfcc's that can be used to compared hfcc's of different regioisomers. Comparison with experiment (vide supra) reinforces this point. The isotropic hyperfine coupling constants were calculated with the help of the Gaussian-98 program.[56]

General Procedures. All cycloaddition reactions were performed under inert atmosphere and in the absence of light. Materials and solvents were obtained from commercial suppliers. C_{60} was purchased from MER corporation (Tucson, AZ). Compounds **1** and **2** were prepared as described in the literature.[10,57]

Instruments. UV-vis: Varian Cary 5; EPR: X-Band Bruker ESP 300 E, equipped with a temperature controller ER 412HT, a field frequency (F/F) lock accessory and built-in NMR

(43) Kriste B. EPRFTSM Program, Freie Universität Berlin, 1991; *J. Magn. Reson.* **1987**, *73*, 213

(44) Dewar, M. J. S.; Zoebisch, E. G.; Healy, E. F.; Stewart, J. J. P. *J. Am. Chem. Soc.* **1985**, *107*, 3902.

(45) AMPAC 6.55, 1997 Semichem, 7204 Mullen, Shawnee, KS 66216.

(46) Solà, M.; Mestres, J.; Martí, J.; Duran, M. *Chem. Phys. Lett.* **1994**, *231*, 325.

(47) Mestres, J.; Duran, M.; Solà, M. *J. Phys. Chem.* **1996**, *100*, 7449.

(48) Luque, F. J.; Bachs, M.; Orozco, M. *J. Comput. Chem.* **1994**, *15*, 847. Bachs, M.; Luque, F. J.; Orozco, M. *J. Comput. Chem.* **1994**, *15*, 446. Orozco, M.; Bachs, M.; Luque, F. J. *J. Comput. Chem.* **1995**, *16*, 563.

(49) Luque, F. J.; Zhang, Y.; Aleman, C.; Bachs, M.; Gao, J.; Orozco, M. *J. Phys. Chem.* **1996**, *100*, 4269.

(50) (a) Miertuš, S.; Scrocco, E.; Tomasi, J. *Chem. Phys.* **1981**, *55*, 117. (b) Tomasi, J.; Persico, M. *Chem. Rev.* **1994**, *94*, 2027.

(51) Stewart, J. J. P. MOPAC6, QCPE 455, Indiana University. Bloomington, IN 1993.

(52) (a) Hohenberg, P.; Kohn, W. *Phys. Rev. A* **1964**, *136*, 864. (b) Kohn, W.; Sham, V. *Phys. Rev. A* **1965**, *140*, 1133.

(53) (a) Becke, A. D. *J. Chem. Phys.* **1993**, *98*, 5648. (b) Lee, C.; Yang, W.; Parr, R. G. *Phys. Rev. B* **1988**, *37*, 785. (c) Stevens, P. J.; Devlin, F. J.; Chablowski, C. F.; Frisch, M. J. *J. Phys. Chem.* **1994**, *98*, 11623.

(54) (a) Binkley, J. S.; Pople, J. A.; Hehre, W. J. *J. Am. Chem. Soc.* **1980**, *102*, 939. (b) Gordon, M. S.; Binkley, J. S.; Pople, J. A.; Pietro, W. J.; Hehre, W. J. *J. Am. Chem. Soc.* **1982**, *104*, 2797.

(55) (a) Adamo, C.; Barone, V.; Fortunelli, A. *J. Phys. Chem.* **1994**, *98*, 8648. (b) Barone, V.; Bencini, A.; di Mateo, A. *J. Am. Chem. Soc.* **1997**, *119*, 10831. (c) Cirujeda, J.; Vidal-Gancedo, J.; Jürgens, O.; Mota, F.; Novoa, J. J.; Rovira, C.; Veciana, J. *J. Am. Chem. Soc.* **2000**, *122*, 11393.

(56) Frisch, M. J.; Trucks, G. W.; Schlegel, H. B.; Scuseria, G. E.; Robb, M. A.; Cheeseman, J. R.; Zakrzewski, V. G.; Montgomery, J. A.; Stratmann, R. E.; Burant, J. C.; Dapprich, S.; Milliam, J. M.; Daniels, A. D.; Kudin, K. N.; Strain, M. C.; Farkas, O.; Tomasi, J.; Barone, V.; Cossi, M.; Cammi, R.; Mennucci, B.; Pomelli, C.; Adamo, C.; Clifford, S.; Ochterski, J.; Petersson, G. A.; Ayala, P. Y.; Cui, Q.; Morokuma, K.; Malick, D. K.; Rabuck, A. D.; Raghavachari, K.; Foresman, J. B.; Cioslowski, J.; Ortiz, J. V.; Stefanov, B. B.; Liu, G.; Liashenko, A.; Piskorz, P.; Komaromi, I.; Gomberts, R.; Martin, R. L.; Fox, D. J.; Keith, T. A.; Al-Laham, M. A.; Peng, C. Y.; Nanayakkara, A.; Gonzalez, C.; Challacombe, M.; Gill, P. M. W.; Johnson, B. G.; Chen, W.; Wong, M. W.; Andres, J. L.; Head-Gordon, M.; Replogle, E. S.; Pople, J. A. Gaussian Inc., Pittsburgh, PA, 1998.

(57) Llacay, J.; Mata, I.; Molins, E.; Rovira, C.; Veciana, J. *Adv. Mater.* **1998**, *10*, 330.

gaussmeter; LDI-TOF: Kratos Kompact Maldi 2 K-probe (KRATOS Analytical) operating with pulsed extraction of the ions; ^{1}H NMR and ^{13}C NMR: Bruker AC 400 and a Bruker Aspect 3000; HMBC NMR: VXR-500S Spectrometer; HPLC: Shimadzu SCL-10A VP, KROMASIL 100 Si 5 μm (Analytical HPLC: Spherisorf 25 × 0.46 cm, 20 μL; Preparative HPLC: Spherisorf 25 × 1.0 cm, 500 μL).

Bis[1,2-(cyclohexenylbismethoxycarbonyltetrathiafulvalene)]-buckminster- fullerene 3. Method A. To a refluxing solution of 73.6 mg (0.1 mmol) of C_{60} in toluene was added a solution of 41 mg (0.1 mmol) of compound **1** in 8 mL of benzonitrile, and the resulting solution was refluxed for 1 h. The solvent was evaporated and the residue chromatographed (silica gel, CS_2−CH_2Cl_2) to give unreacted C_{60} (15 mg, 20.4% from the initial C_{60}), 60 mg of monoadduct **2** (69.1% from reacted C_{60}), and 33 mg of a mixture of bisadducts **3** (28.7% from reacted C_{60}).

Method B. A solution of 200 mg (0.18 mmol) of monoadduct **2** and 38 mg (0.09 mmol) of compound **1** in 40 mL of cholorobenzene was refluxed for 1 h. The solvent was evaporated and the residue chromatographed (silica gel, CH_2Cl_2) to give 124 mg of unreacted monoadduct (62% from initial monoadduct **2**) and 58 mg of a mixture of bisadducts **3** (57.7% from reacted monoadduct **2**).

FT-IR (KBr) υ (cm^{-1}) 1734, 1576, 1433, 1258, 1090, 1026, 766, 527; UV-vis (CH_2Cl_2) λ_{max}(log ϵ) 257 (4.96), 310 sh. (4.72), 418 sh. (3.88), 450 sh. (3.77), 675−750 broad band (1.30); HRMS calcd for $C_{84}H_{20}O_8S_8$ m/z 1411.892, found 1411.892; LDI-TOF-MS 1412 [M$^+$]; ^{1}H NMR (300 MHz, CS_2−CD_2Cl_2 1:2) δ (ppm) 4.31−4.25 (m, broad), 3.91−3.87 (m).

Generation of Radical Cations and Anions Derived from 3. Radical cations were obtained by in situ electrochemical reduction, monitored by an EG&G PAR 263A potentiostat/galvanostat, on an EPR cell equipped with Pt wires as working and counter electrodes and using the Ag/AgCl system as a reference electrode. Experimental conditions for the electrochemical generation of radical cations was as follows: +0.8 V, CH_2Cl_2 0.2 M in Bu_4NPF_6. Experimental conditions for the electrochemical generation of radical anions was as follows: −0.8 V, CH_2Cl_2 0.2 M in Bu_4NPF_6.

Acknowledgment. We are indebted to Prof. F. J. Luque and Prof. M. Orozco for a copy of their MST coded implemented in the MOPAC program. Financial help has been furnished by the Spanish DGES (PB98-0457-C02-01, BQU200-1157, and PB97-0933) and CIRIT (2000 SGR 00114). M.M.T. is grateful to the Generalitat de Catalunya for a pre-doctoral grant. M. S. is indebted to the Departament d'Universitats, Recerca i Societat de la Informació of the Generalitat de Catalunya for financial support through the Distinguished University Research Promotion 2001.

Supporting Information Available: Complete computational details in the form of Z-matrixes for the theoretical studies carried out for isomers of **3**. This material is available free of charge via the Internet at http://pubs.acs.org.

JO010748F

COMUNICACIÓ C

Títol: A New Family of Conducting and Magnetic Charge-Transfer Salts from BMDT-TTF.

Autors: M. Mas-Torrent, S. S. Turner, K. Wurst, J. Vidal-Gancedo, J. Veciana, C. Rovira, P. Day.

Publicació: *Synth. Met*., 120, 799-800.

Any: 2001

ELSEVIER

Synthetic Metals 120 (2001) 799–800

SYNTHETIC METALS

www.elsevier.com/locate/synmet

A new family of conducting and magnetic charge-transfer salts from BMDT-TTF

M. Mas-Torrent[a], S.S. Turner[b], K. Wurst[c], J. Vidal-Gancedo[a], J. Veciana[a], C. Rovira[a*], P. Day[b*]

[a] *Institut de Ciència de Materials de Barcelona (CSIC), Campus Universitari, 08193 Bellaterra, Catalunya, Spain*
[b] *The Royal Institution of Great Britain, Davy Faraday Research Laboratory, 21 Albemarle St. W1X 4BS London, UK*
[c] *Institut für Allgemeine Anorgan. und Theoret. Chemie, Univ. Innsbruck, Innrain 52a, A-6020 Innsbruck, Austria*

Abstract

Crystals suitable for X-ray structure determination have been obtained from the electrocrystallisation of BMDT-TTF donor, bis(methylenedithio)tetrathiafulvalene, with (N-quinolinium)[$Cr(NCS)_4(quinoline)_2$], although, due to a ligand exchange during the electrocrystallisation, it has been found that the product is in fact $(BMDT\text{-}TTF)_4[Cr(NCS)_6]$. In this salt the anions and the donors form segregated layers. A salt from BMDT-TTF and (N-isoquinolinium)[$Cr(NCS)_4(isoquinoline)_2$] has also been prepared. Raman, EPR and NIR measurements have also been carried out.

Keywords: Organic conductors, electrocrystallisation, electron spin resonance, X-ray diffraction, magnetic measurements, raman spectrometry.

1. Introduction

Establishing superconductivity in a crystal lattice containing localised electrons is a desirable aim because superconductivity and magnetism have long been considered inimical to each other. However, because of the well-defined separation between the organic and inorganic components in the charge transfer salts of BEDT-TTF (bis(ethylenedithio)tetrathiafulvalene) and $[M^{III}(C_2O_4)_3]^{3-}$ (M = Fe, Co, Cr), it has been found that these two properties can coexist in these compounds. Thus, the first molecular superconductor containing localised magnetic moments, $(BEDT\text{-}TTF)_4[(H_3O)Fe(C_2O_4)_3].C_6H_5CN$, was reported[1]. More recently, new charge transfer salts with TTF and BEDT-TTF with the counter ions $[M(NCS)_4(isoquinoline)_2]^-$ (M=Cr, Fe) have been described, which display long range ferrimagnetic order[2].

In this communication we present the results from the study of two new charge transfer salts formed by the electrocrystallisation of BMDT-TTF (bis(methylene-dithio)tetrathiafulfalene) and the magnetic anions $[N\text{-donor}]^+[Cr(NCS)_4(N\text{-donor})_2]^-$ (N-donor = quinoline or isoquinoline).

2. Experimental

The synthesis of BMDT-TTF was performed as previously described[3] whereas the salts with the magnetic anions were obtained by a ligand exchange reaction from Reinecke's salt, $NH_4[Cr(NCS)_4(NH_3)_2]$, on adding the corresponding N-donor compound and refluxing in ethanol overnight[2]. The electrochemical crystal growth of the charge transfer salts was carried out from dichloromethane solutions in conventional H-shaped cells with Pt electrodes at a constant temperature (295(2) K) over one week and at a constant current of 1 μA. For both quinoline and isoquinoline salts black needles were obtained.

3. Results and Discussion

The optical absorption spectra of the salt obtained using quinoline as N-donor **1** shows the "A" band, typical of a partial oxidation of the donor, centred at around 3550 nm (Fig.1). However, this band is not present in the salt obtained from the isoquinoline compound **2**, which implies that it should be a completely ionic salt.

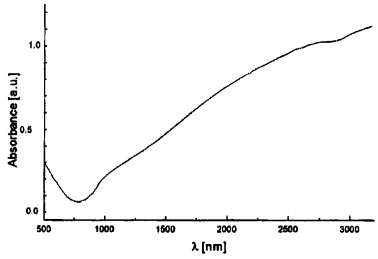

Fig. 1. NIR spectrum for **1**.

* P. Day: e-mail pday@ri.ac.uk ; C. Rovira: e-mail cun@icmab.es

PII: S0379-6779(00)01010-9

The elemental analysis of **2** can be fitted to the molecular formula (BMDT-TTF)][Cr(NCS)$_4$(isoquinoline)$_2$].H_2O, which is in agreement with the fact that the donor is totally oxidised. On the other hand, single crystals good enough for X-ray diffraction of **1** were obtained and the crystal structure was determined[4]. This salt crystallised in the centrosymmetric space group $C_{2/c}$ with segregated donor and acceptor layers alternating along c axis (Fig.2). Surprisingly, the molecular formula of the salt is (BMDT-TTF)$_4$[Cr(NCS)$_6$], and quinoline is not present. This can only be explained by a ligand exchange during the electrocrystallisation due to the quinoline lability.

a)

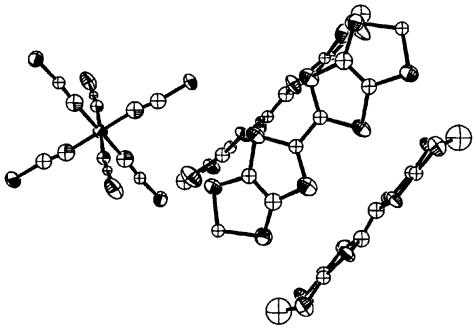

b)

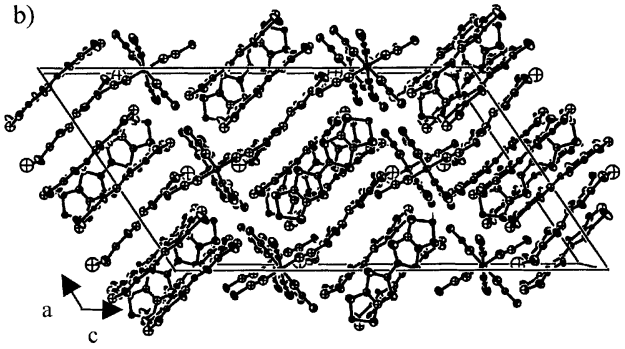

Fig. 2. Crystal structure of **1**. a) Growth unit. b) Crystal packing.

The degree of ionicity of the donor in both salts has been studied by Raman Spectrometry since it has previously been described that there is an approximately linear dependence between the ionicity and the Raman-active C=C stretching frequencies in salts of the electron-donor molecule BEDT-TTF[5]. Raman spectra of BMDT-TTF neutral donor shows two bands at 1501.9 and 1549.7 cm^{-1} in the C=C stretching region, while in salt **1** we can observe one band at 1438.6 cm^{-1} and in salt **2** one at 1432.6 cm^{-1}. Fitting those data with the equations used with BEDT-TTF, the ionicity of 0.75 and 0.8 was found for salts **1** and **2** respectively. Salt **1** Raman results agree with the molecular formula, but for salt **2** it doesn't correspond with the expected 1:1 stoichiometry, which can be due to the fact that there are hydroxonium cations in the structure.

The SQUID measurements of salt **2** show that it is paramagnetic and its susceptibility can be fitted to a Curie–Weiss law over all temperatures (2-300 K) with almost ideal Curie constant for high spin Cr(III) (1.918) and small negative Weiss constant (-4.779).

In the Electron Spin Resonance spectrum of **1** we can observe a broad signal with a linewidth of 320 G and a g factor of 2.0134. The temperature dependence of the EPR signal has been studied down to 108 K and no important changes in its parameters have been observed, revealing that there are no phase transitions (Fig. 3).

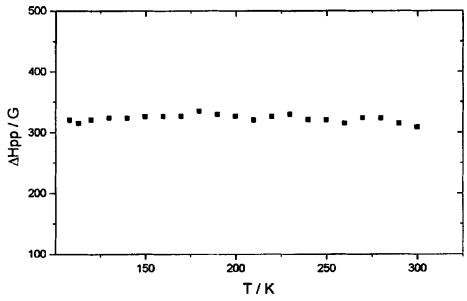

Fig 3. Temperature dependence of ΔHpp of EPR signal of **1**.

Work is now in progress in order to obtain better crystals to study the transport properties and the influence of the conducting electrons on the magnetism.

Acknowledgements. This work was supported by the grants from the EC [TMR, ERBFMRX-CT980181 and COST D14/0003/99] and DGES, Spain [PB96-0872-01].

References

[1] a) A. W. Graham, M. Kurmoo, P. Day, J. Chem. Soc. Chem. Commun., (1995) 2061. b) M. Kurmoo, A. W. Graham, P. Day, S. J. Coles, M. B. Hursthouse, J. L. Caufield, J. Singleton, F. L. Pratt, W. Hayes, L. Ducasse, P. Guionneau, J. Am. Chem. Soc., (1995) 12209.

[2] S. S. Turner, C. Michaut, S. Durot, P. Day, T. Gelbrich, M. B. Hurtshouse, J. Chem. Soc. Dalton Trans., 6 (2000) 905.

[3] R. Kato, Y. Sasaki, H. Kobayashi, Chem. Lett., (1984) 993.

[4] Crystallographic data for $C_{38}H_{16}CrN_6S_{38}$: crystal dimensions 0.2x0.1x0.02 mm; M_r = 1827.09, monoclinic, space group $C_{2/c}$, a=37.235, b=10.054, c=21.063, β=124.23; V =6519.34.

[5] H. Hwang, J. R. Ferraro, J. M. Williams, U. Geiser, J. A. Schlueter, J. Chem. Soc. Chem. Commun., (1994) 1893.

ARTICLE D

Títol: New Flexible Low Density Metallic Materials Containing the $(BEDT\text{-}TTF)_2(I_xBr_{1-x})_3$ Molecular Metals as Active Components.

Autors: E. Laukhina, V. Tkacheva, I. Chuev, E. Yagubskii, J. Vidal-Gancedo, M. Mas-Torrent, C. Rovira, J. Veciana, S. Khasanov, R. Wojciechowski J. Ulanski.

Publicació: *J. Phys. Chem. B*, 105, 11089-11097.

Any: 2001

New Flexible Low-Density Metallic Materials Containing the $(BEDT\text{-}TTF)_2(I_xBr_{1-x})_3$ Molecular Metals as Active Components

Elena Laukhina,*,†,‡,§ Vladeslava Tkacheva,‡ Igor' Chuev,‡ Eduard Yagubskii,‡ Jose Vidal-Gancedo,† Marta Mas-Torrent,† Concepció Rovira,*,† Jaume Veciana,† Salavat Khasanov,*,|| Roman Wojciechowski,⊥ and Jacek Ulanski⊥

Institut de Ciencia de Materials de Barcelona, CSIC, Campus UAB, E-08193 Bellaterra, Spain, IPCP RAS, 142432, Chernogolovka, MD, Russia, ISSP RAS, 142432, Chernogolovka, MD, Russia, and Department of Molecular Physics, Technological University of Lodz, 90-924, Lodz, Poland

Received: April 18, 2001; In Final Form: August 15, 2001

New conducting bilayer films (BL-film) containing $(BEDT\text{-}TTF)_2(I_xBr_{1-x})_3$ molecular metals as active components have been prepared. The effect of various parameters of the BL-film preparation on the conducting layer composition was systematically studied by X-ray, Raman, EPR, and SEM. It was shown that the conducting layer of new BL-films is formed by "*c*" oriented $(BEDT\text{-}TTF)_2(I_xBr_{1-x})_3$ nanocrystals which contain a set of the IBr_2^-, I_2Br^-, and/or I_3^- anions. It was found that the $\alpha' \rightarrow \beta$ phase transition takes place in the $(BEDT\text{-}TTF)_2(I_xBr_{1-x})_3$ nanocrystals under film annealing. Some of the new composite BL-films, being flexible and transparent, reveal a metal-like temperature dependence of resistance down to nitrogen temperature.

1. Introduction

Polymeric composite films[1−4] containing a thin layer of organic conductors are very attractive as conducting materials for a novel generation of devices which can gain the unusual electronic properties of molecular metals.[5] These composite bilayer (BL) films demonstrate different transport properties[1,6,7] retaining the advantageous properties of the polymeric matrix such as flexibility, transparency and low density. We have reported an unique BL-film featuring a metallic behavior of resistance over the whole temperature range studied and revealing superconducting properties below 5−7 K.[1,8] This material contains a conducting surface layer formed by the linked microcrystals of the organic superconductor β_t-$(BEDT\text{-}TTF)_2I_3$ (BEDT-TTF = bis(ethylenedithio)tetrathiafulvalene).[9,10] Other flexible and transparent BL-films with a very thin conducting surface layer of BET/I_3,[3] $(BEDO\text{-}TTF)_{2.4}I_3$, or β-$(BEDO\text{-}TTF)_2Br{\cdot}3H_2O$[6] microcrystals (BET-TTF = bis(ethylenethio)tetrathiafulvalene; BEDO-TTF = bis(ethylenedioxo)tetrathiafulvalene) also demonstrate metal-like transport properties in a wide temperature region. The above BL-films can be successfully prepared by the modified reticulate doping technique (MRDT).[1,4,8] During the progress of our research, we have extended the MRDT for the preparation of new conducting BL-films with a conducting surface layer formed by nanocrystals of $(BEDT\text{-}TTF)_2(I_xBr_{1-x})_3$ molecular metals. These new transparent flexible films are conductors in a wide temperature region, some of them revealing a metal-like behavior of resistance down to nitrogen temperature.

Here we present the preparation of new conducting BL-films containing $(BEDT\text{-}TTF)_2(I_xBr_{1-x})_3$ molecular conductors as active components and the effect of various conditions of MRDT on the structure and texture of the $(BEDT\text{-}TTF)_2(I_xBr_{1-x})_3$ conducting layers. Additionally, the details of the $\alpha' \rightarrow \beta$ structural phase transition of the new $(BEDT\text{-}TTF)_2(I_xBr_{1-x})_3$ molecular conductors under film annealing and the transport properties of all new conducting BL-films in a wide temperature region are also outlined in this paper.

2. Experimental Section

A. Film Preparation. Polycarbonate (PC) films (10−15 μm thickness) containing 2 wt % of molecularly dispersed BEDT-TTF were made by casting the solution of PC (≅1 g) and BEDT-TTF (0.02 g) in 1,2-dichlorobenzene (≈50 mL) at t = 130 °C as previously described[2,7] (first stage, Scheme 1). Then the

SCHEME 1: Scheme of MRDT Used for the Preparation of New Conducting BL-Films with the Conducting Layer of the β_t-$(BEDT\text{-}TTF)_2(I_xBr_{1-x})_3$ Nanocrystals

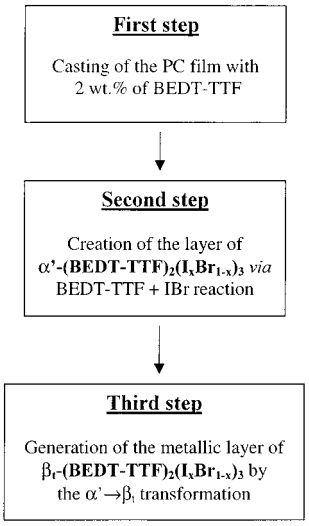

* To whom correspondence should be addressed. ICMAB Campus UAB, E-08193 Bellaterra, Spain. FAX: (34)93 580 57 29. E-mail: vladimir@icmab.es and cun@icmab.es.
† Institut de Ciencia de Materials de Barcelona.
‡ IPCP RAS.
§ Permanent address: IPCP RAS, 142432, Chernogolovka, MD, Russia.
|| ISSP RAS.
⊥ Department of Molecular Physics.

10.1021/jp011470y CCC: $20.00
Published on Web 10/23/2001

TABLE 1: Parameters of the Second Step Used for the Film Samples Preparation

film sample	temp, °C	$C_{IBr/s}$, M	time period of the treatment, min
1	23	0.024	2
2	23	0.024	4
3	23	0.024	6
4	23	0.024	10
5	25	0.036	2
6	25	0.036	4
7	25	0.036	6
8	23	0.048	2
9	23	0.048	4
10	23	0.048	6

surface of the PC/ BEDT-TTF film was treated with vapor of a IBr/CH_2Cl_2 solution during different time periods (Table 1), which provided a way to form a conducting surface layer with the α′-$(BEDT\text{-}TTF)_2(I_xBr_{1-x})_3$ nanocrystals (second step, Scheme 1). During the second step we used a binary mixture system: IBr/CH_2Cl_2 solution−IBr/CH_2Cl_2 vapor at equilibrium. The mole fraction of IBr contained in a IBr/CH_2Cl_2 solution (x^*_{IBr}) was always much greater than the mole fraction of BEDT-TTF ($x^*_{BEDT-TTF}$) contained in the swollen surface layer of the film. All time periods used for the film surface treatment were not sufficient to achieve the saturation of the swollen layer of the film with IBr. Afterward, all the BL-films were annealed at 155−160 °C during 3 h to form the β_t-$(BEDT\text{-}TTF)_2(I_xBr_{1-x})_3$ conducting layer (third step, Scheme 1). To prevent a degradation of the nanocrystals during the BL-film annealing, the conducting surface of the film samples has to be protected sandwiching them between two glass plates. To provide a protective coat for the conducting surface layer, we also successfully used an aluminum foil.

B. BL-Film Characterization. X-ray diffraction patterns have been measured using Siemens D-500 diffractometer in the reflection mode.

The Raman spectra of the composite films were recorded at room temperature using Jobin-Yvon T64000 MicroRaman spectrometer, working in a backscattering mode. The measurements were performed with 632 nm laser line and with spectral resolution of 1 cm^{-1}. Diamond (1332 cm^{-1}) and silicon (520 cm^{-1}) lines were used for the calibration of the spectrometer. Two typical Raman spectra of the film samples are depicted in Figure 1.

EPR spectra were recorded using Bruker WSP-300E spectrometer operating in the X-band (9.5 GHz) with a rectangular TE 102 cavity and equipped with a field-frequency (F/F) lock accessory and a built-in Bruker NMR gaussmeter ER 035 M. Heating was made with a rate of 1°/min in a Bruker ER 4121 HT nitrogen cryostat (100−500 K) (see Figure 2.) Rotations were performed by means of a Bruker programmable goniometer ER 218 PGl 8 (see Figure 3). Precautions to avoid undesirable spectral line broadening, such as that arising from microwave power saturation and magnetic field overmodulation, were taken.

The morphology of conducting surface layers was investigated using a scanning electron microscope (SEM) operating at 20 kV. The SEM micrographs of BL films **1**, **7**, and **8** are presented in Figure 4.

Temperature resistance dependencies were measured down to 1.5 K using a standard 4-probe dc-method. Four annealed platinum wires (20 μm in diameter) were attached to the conducting surface of a BL-film by a conductive graphite paste. The scheme of a film sample montage is presented as an insert of Figure 5.

3. Results and Discussion

To gain a better understanding of the possibilities and restrictions of MRDT, it is very important to clarify the real processes that take place during the BL-film preparation. Thus, what kind of conducting nanocrystals can be formed at the second step via BEDT-TTF + IBr reaction is certainly a question to answer. Undoubtedly, the thermodynamic consideration of the BEDT-TTF + IBr reaction have to be useful to clarify the problem.

A. Chemical Reactions Due to the BEDT-TTF and IBr Interaction. Ab Initio Estimation and Effect of the Experimental Parameters. Below we will focus on the consideration of chemical reactions which can occur in the swollen surface layer of the PC/BEDT-TTF film at the second step of MRDT (Scheme 1). Assuming that the nanocrystals of the conducting layer are formed under a steady chemical reaction, we can estimate the probability P of each plausible BEDT-TTF + IBr reaction on the basis of Boltzmann distribution $p \sim \exp(-E/RT)$, where E is energy, R is the universal gas constant, and T is temperature. The analysis of all the possible results of the BEDT-TTF + IBr interaction producing species such as $I^{\pm1,0}$, $I_2^{\pm1,0}$, $I_3^{\pm1,0}$, $IBr^{\pm1,0}$, $Br^{\pm1,0}$, $Br_2^{\pm1,0}$, $Br_3^{\pm1,0}$, $IBr_2^{\pm1,0}$, and $I_2Br^{\pm1,0}$, allows us to restrict the set of the most energetically favorable reactions, which result in the maximum (2-fold) enhancement of the number of new bonds, by a factor of five:

$$8BEDT\text{-}TTF + 6IBr \leftrightarrow [8(BEDT\text{-}TTF)]^{+4} + 2I_2Br^- + 2IBr_2^- \quad (1)$$

$$8BEDT\text{-}TTF + 6IBr \leftrightarrow [8(BEDT\text{-}TTF)]^{+4} + I_3^- + 3IBr_2^- \quad (2)$$

$$8BEDT\text{-}TTF + 6IBr \leftrightarrow [8(BEDT\text{-}TTF)]^{+4} + Br_3^- + 3I_2Br^- \quad (3)$$

$$8BEDT\text{-}TTF + 6IBr \leftrightarrow [8(BEDT\text{-}TTF)]^{+4} + 2I_3^- + 2Br_3^- \quad (4)$$

$$8BEDT\text{-}TTF + 6IBr \leftrightarrow [8(BEDT\text{-}TTF)]^{+4} + I_3^- + I_2Br^- + IBr_2^- + Br_3^- \quad (5)$$

The energy of the reactions was calculated on the basis of an additive approach. It means that intermolecular interactions of the reagents were not taken into consideration. For all these reactions, we have compared only the energies of the species formed due to the reduction of IBr, since the contributions of the others species are constant. Ab initio calculations (Table 2) have been carried out on the MP2/LANL2DZ level (GAUSSIAN94).[11] The effect of the solvent (nitrobenzene) was calculated according to the Onsager model.[12] We were especially interested in the estimation of the effect of nitrobenzene since we had already found that the β-type crystals which were synthesized in nitrobenzene via BEDT-TTF + IBr reaction[13] contain the assembly of I_3^-, I_2Br^-, and IBr_2^- anions.[14] On the basis of the calculations tabled in Table 2, the probability of the reactions 3−5 equals zero. Thus, for the BEDT-TTF + IBr reaction (second step of MRDT), it would be plausible to suggest the formation of the I_3^-, I_2Br^-, and IBr_2^- trihalide anions only. We have also estimated the contribution of each of these trihalide anions in vacuum and nitrobenzene. These data are summarized in Table 3. According to these results, the anion composition of the above-mentioned single crystals obtained in nitrobenzene can be formulated as $[(I_3)_{0.07}(I_2Br)_{0.37}(IBr_2)_{0.56}]^-$

TABLE 2: Energy of Changing Species *E* in the Proposed BEDT-TTF + IBr Reaction and Boltzmann Probability *P* of This Reaction in Vacuum (v) and in Nitrobenzene (s)

reaction	E_v, au	P_v	E_s, au	P_s
1	−145.250	0.5	−145.339	0.74
2	−145.250	0.5	−145.338	0.26
3	−145.237	0	−145.318	0
4	−145.224	0	−145.294	0
5	−145.237	0	−145.317	0

TABLE 3: Contribution *C* of Trihalide Anions in Vacuum (v) and in Nitrobenzene (s)

anion	C_v,%	C_s,%
I_3^-	12.5	6.5
I_2Br^-	25.0	37.0
IBr_2^-	62.5	56.5

that gives us an average stoichiometry of $I_{1.5}Br_{1.5}$ for the anion. This result is in excellent agreement with EDX data which indicate for this compound the I/Br atomic ratio of 1:1.[13]

In line with the thermodynamic consideration (Tables 2 and 3), one can expect with reasonable confidence that the contribution of each trihalide anion should be different in various organic solvents and depend on the polarity of the environment. Since the polarity of a swollen polymeric matrix depends on different factors (amount of 1,2-dichlorobenzene used at the first step, variation of CH_2Cl_2 concentration with time at the second step and polarity of PC), the contribution of each trihalide anion to the composition of the nanocrystals that form the conducting layers is difficult to estimate quantitatively. Nevertheless, in accordance with the ab initio calculations, we may presume that in the swollen surface of the BL-film samples the $(BEDT\text{-}TTF)_2(I_xBr_{1-x})_3$ nanocrystals containing the majority of the IBr_2^- anions along with smaller amounts of the I_3 and/or I_2Br^- species should be mainly formed. In attempting to estimate the *x* value in the outlined formula, one should also keep in mind that the size of trihalide anions sets limits on the formation of different crystal phases of the BEDT-TTF trihalide family. For example, I_3^- species promote the formation of α-, *β*-, *θ*-, and *κ*-type crystal modifications of the $(BEDT\text{-}TTF)_2I_3$ salt, while smaller IBr_2^- species are beneficial for α′- and *β*-type $(BEDT\text{-}TTF)_2IBr_2$ crystal phases only.[5] Therefore, at the second step via BEDT-TTF + IBr reaction the α′-$(BEDT\text{-}TTF)_2(I_xBr_{1-x})_3$ and/or *β*-$(BEDT\text{-}TTF)_2(I_xBr_{1-x})_3$ crystal phases can be expected to form along with other above crystal modifications. Some amount of amorphous salts with mixed anions can be also formed. Considering all this, the *x* value should depend on the type of the crystal phase and may differ for various nanocrystals. Evidently, to characterize the conducting layer of new BL-film samples, we should determine the type of nanocrystals (BEDT-TTF packing motif) and the composition of the anion as well. We have chosen X-ray, EPR, and Raman spectroscopy as the techniques for the films' characterization, which are the best suited for both outlined requirements.

The reagent ratio at the BEDT-TTF + IBr reaction is also a very important parameter because it determines the formation of trihalide salts with a different charge-transfer degree. We suggest that there is a range of optimum masses of IBr absorbed per unit volume of a swollen film surface layer ($C_{IBr/film}$) at which a conducting layer of $(BEDT\text{-}TTF)_2(I_xBr_{1-x})_3$ nanocrystals is achieved. Generally, the $C_{IBr/film}$ value is proportional to (i) the mass of IBr in the vapors of IBr/CH_2Cl_2 solution ($m_{IBr/v}$) and (ii) the duration of the film surface treatment *t*. According to the gas-state equations[15] and by Henry's law,[15] the $m_{IBr/v}$ value is proportional to the mole fraction of IBr (x_{IBr}*) contained in the IBr/CH_2Cl_2 solution and it can be shown that

$$C_{IBr/film} \cong D_{IBr} C_{IBr/s} V_s t \quad (1)$$

where D_{IBr} is the capability of IBr vapors to penetrate into a swollen polycarbonate layer, $C_{IBr/s}$ is the molar concentration of IBr, and V_s is the volume of IBr/CH_2Cl_2 solution. To find the above range of the $C_{IBr/film}$ optimum values we varied $C_{IBr/s}$ and *t* values (see Table 1); in all experiments the amount of BEDT-TTF, the treated film surface layers (7 cm^2), volumes of vapor (29.5 mL), and solution (10.5 mL) were identical. The second steps were done at the same temperature to fix the following parameters: D_{IBr} values, rate of the reaction, and rate of the reagents' diffusion. Taking into account the outlined particularities of the second step of MRDT, we may restrict ourselves to the simple estimation of the $C_{IBr/film}$ values with the factor F_{IBr} that is proportional to the molar concentration of IBr in CH_2Cl_2 and duration of a film surface treatment (Table 1):

$$F_{IBr} = C_{IBr/s} t \quad (2)$$

By using different concentrations of IBr in IBr/CH_2Cl_2 solutions ($C_{IBr/s}$) and various time periods of a surface treatment, we have prepared different BL-film samples **1**−**10** (Table 1). These conducting BL-films were eventually formed with different F_{IBr} values.

B. Composition and Structure of Conducting Layers after the Second Step of the Film Preparation. The X-ray analysis of BL-film samples indicate the presence in all spectra of only (00*l*) reflections that are characteristic of conducting layers formed by oriented nanocrystals. The *c** axis of the nanocrystals is perpendicular to the film surface and, consequently, their conducting layers are parallel to it. The measured values of the interplanar spacing d_{001} along with intensities of (00*l*) reflections allowed us to identify the different phases of the BEDT-TTF trihalides (Table 4).

While at the highest values of F_{IBr} (film samples **4**, **7**, **9** and **10**) the most intensive reflections correspond to the α′-$(BEDT\text{-}TTF)_2IBr_2$ phase with d_{00l} = 16.32 Å, at the lower F_{IBr} values (film samples **1**−**3**, **5**, **6**, and **8**) the most intensive reflections indicate the existence of the α′ phases with the characteristic values of d_{001} in the range from 16.365(3) to 16.422(3) Å. Since these d_{001} values are higher than those of the α′-$(BEDT\text{-}TTF)_2IBr_2$ single crystal, it may be suggested that the conducting layer of samples **1**−**3**, **5**, **6**, and **8** consists of α′-type nanocrystals with an anion layer which should contain the IBr_2^- species along with bigger trihalide anions such as I_3^- and/or I_2Br^-. Thus, X-ray data show that the conducting layer of BL-films produced at the lowest F_{IBr} values consists of the α′-$(BEDT\text{-}TTF)_2(I_xBr_{1-x})_3$ nanocrystals ($0.66 > x > 0.33$) containing different sets of the IBr_2^-, I_2Br^-, and I_3^- trihalide anions. These X-ray data are in agreement with the thermodynamic consideration of the BEDT-TTF + IBr interaction (see above). It should be noted that the X-ray diffraction patterns of samples **2**, **3** also demonstrate extra small reflections corresponding to the *β* phase of BEDT-TTF salts.[5,13] In the X-ray diffraction patterns of samples **3**, **4**, **9**, and **10** the extra reflections correspond to a new BEDT-TTF trihalide salt (N-salt) with d_{001} = 33.30(1) Å (Table 4). While according to X-ray data the metallic *β*-$(BEDT\text{-}TTF)_2(I_xBr_{1-x})_3$ nanocrystals with the value of *x* equal to 0.70(5) (sample **2**) or 0.61(5) (sample **3**) are formed in a small amount, the contribution of the N-salt can be significant especially in the BL-film samples prepared at the highest F_{IBr} values (F_{IBr} = 24 M min, sample **4**, and F_{IBr} = 28.8 M min, sample **10**). The formation of the N-salt is undesirable from the viewpoint of the electrical properties of

TABLE 4: Composition of the Conducting Layer of the Films after the Second Step of the Film Preparation

sample	F_{IBr} 10^{-2}, M min	X-ray data			conducting layer composition[a]
		d_{00l}, Å	phase	$(I_xBr_{1-x})_3$	
			At $C_{IBr/s}$ = 0.024 M		
1	4.8	16.402(3)	α′	$0.66 > x > 0.33$	α′-(BEDT-TTF)$_2$(I$_3$)$_y$ (I$_2$Br)$_z$(IBr$_2$)$_{1-y-z}$
2	9.6	16.407(3)	α′	$0.66 > x > 0.33$	α′-(BEDT-TTF)$_2$(I$_3$)$_y$(I$_2$Br)$_z$(IBr$_2$)$_{1-y-z}$
		15.04(1)	β	$x = 0.70(5)$	β-(BEDT-TTF)$_2$(I$_3$)$_y$ (I$_2$Br)$_z$(IBr$_2$)$_{1-y-z}$
		16.365(3)	α′	$0.66 > x > 0.33$	
3	14.4	15.02(1)	β	$x = 0.61(5)$	α′-(BEDT-TTF)$_2$(I$_3$)$_y$ (I$_2$Br)$_z$(IBr$_2$)$_{1-y-z}$,
		33.32(1)	new		β-(BEDT-TTF)$_2$(I$_3$)$_y$ (I$_2$Br)$_z$(IBr$_2$)$_{1-y-z}$
					N-salt
4	24.0	16.320(5)	α′	$x = 0.33$	
		33.32(1)	new		α′-(BEDT-TTF)$_2$IBr$_2$ and
					N-salt
			At $C_{IBr/s}$ = 0.036 M		
5	7.2	16.422(2)	α′	$0.66 > x > 0.33$	α′-(BEDT-TTF)$_2$ (I$_2$Br)$_y$(IBr$_2$)$_{1-y}$
6	14.4	16.380(3)	α′	$0.66 > x > 0.33$	α′-(BEDT-TTF)$_2$ (I$_2$Br)$_y$(IBr$_2$)$_{1-y}$
7	21.6	16.325(5)	α′	$x = 0.33$	α′-(BEDT-TTF)$_2$IBr$_2$
			At $C_{IBr/s}$ = 0.048 M		
8	9.6	16.380(3)	α′	$x > 0.33$	α′-(BEDT-TTF)$_2$ (I$_2$Br)$_y$(IBr$_2$)$_{1-y}$
9	19.2	16.31(1)	α′	$x = 0.33$	
		33.26(4)	new		α′-(BEDT-TTF)$_2$IBr$_2$
					N-salt
10	28.8	16.317(4)	α′	$x = 0.33$	α′-(BEDT-TTF)$_2$IBr$_2$ and
		33.30(1)	new		N-salt

[a] The anion composition of nanocrystals was determined by Raman spectroscopy (see Table 5).

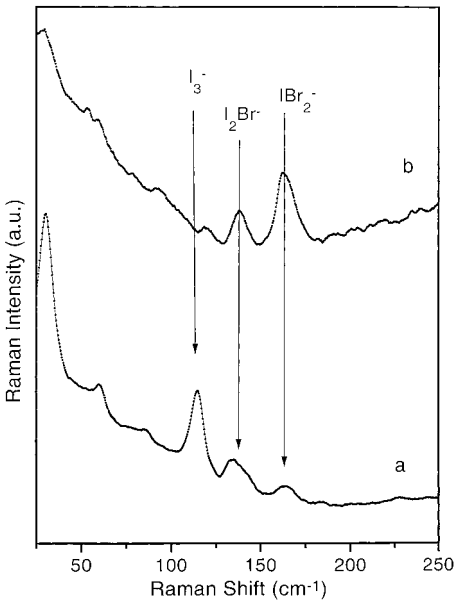

Figure 1. Raman spectra of film samples (a) **1** and (b) **7** containing the conducting layer of the α′-(BEDT-TTF)$_2$(I$_x$Br$_{1-x}$)$_3$ nanocrystals.

BL-films (see below). The X-ray results indicate that at the second step of MRDT via BEDT-TTF + IBr reaction two types of conducting layers can be formed: (i) conducting layers containing only α′-type nanocrystals and (ii) conducting layers consisting of different BEDT-TTF trihalide salts. Therefore, at the second step of MRDT we have a good chance to achieve the optimum $C_{IBr/film}$ value which is favorable to the generation of an uniform surface conducting layer composed of only the α′ phase of BEDT-TTF trihalide salts.

It has been demonstrated by both ab initio calculations and Raman studies of single crystals[14] that Raman spectra can be successfully used to clarify the $(I_xBr_{1-x})_3^-$ anion composition by observing the distinct halogen vibrations of the trihalide anions in the range of 100−200 cm^{-1}. Low-frequency Raman measurements were therefore performed in order to define which types of trihalide anions are included in the anion layer of the

TABLE 5: Data of Low-Frequency Raman Spectra of the BL-Film Samples with the Conducting Layer Formed during the Second Step of MRDT

BL-film sample	Raman ν, cm^{-1} [a]	assignment
1	115 s	υ^b I_3^-
	135 m	υ I_2Br^-
	164 w	υ IBr_2^-
2	115 m	υ I_3^-
	135 m	υ I_2Br^-
	164 m	υ IBr_2^-
3	115 vw	υ I_3^-
	135 m	υ I_2Br^-
	164 m	υ IBr_2^-
4	135 vw	υ I_2Br^-
	164 m	υ IBr_2^-
5	115 m	υ I_3^-
	135 m	υ I_2Br^-
	164 m	υ IBr_2^-
6	135 w	υ I_2Br^-
	164 m	υ IBr_2^-
7	135 vw	υ I_2Br^-
	164 m	υ IBr_2^-
	135 m	υ I_2Br^-
8	164 s	υ IBr_2^-
9	135 vw	υ I_2Br^-
	164 m	υ IBr_2^-
10	164 m	υ IBr_2^-

[a] Relative intensities: s = strong, m = medium, w = weak, vw = very weak. [b] υ is a symbol used for stretching vibrations of a trihalide anion.

α′-, β-, and N-type nanocrystals. In this frequency range the quality of the Raman spectra of film samples studied are enough to detect Raman bands as well as to assign them to vibrations of either I_3^-, I_2Br^-, or IBr_2^- anions (Figure 1, Table 5). The low-frequency Raman spectra of samples **1**−**3** and **5** shows the band at 115 cm^{-1} due to the stretching vibration of I_3^- anions and two bands at 135 and 164 cm^{-1} resulting from the stretching vibrations of the I_2Br^- and IBr_2^- anions, respectively.[14,17] The Raman spectra of samples **4** and **6**−**9** show only the two bands of the stretching vibrations of the I_2Br^- and IBr_2^- linear anions, while the stretching vibration of sample **10** shows only a band due to the IBr_2^- species. These results are in excellent agreement

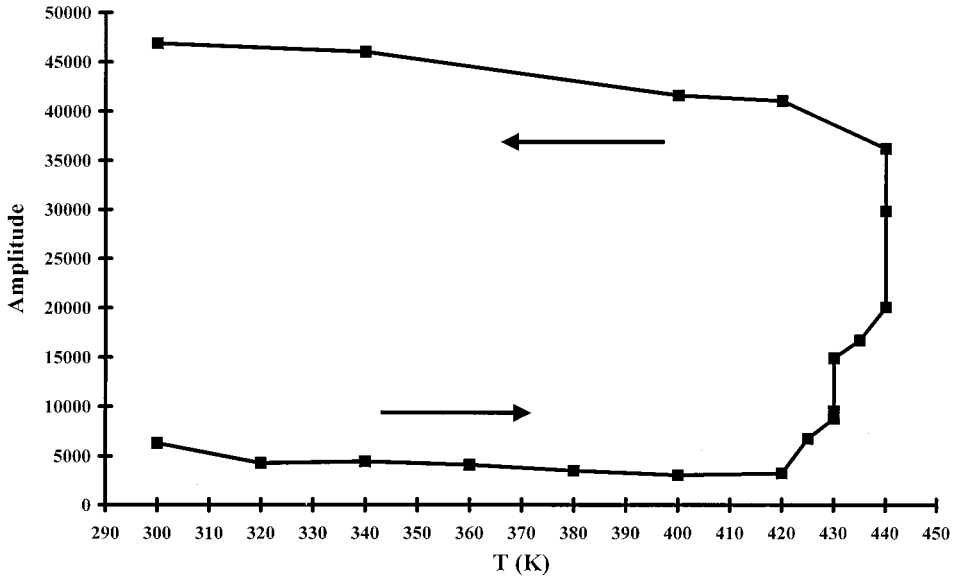

Figure 2. Temperature dependence of the EPR signal amplitude for sample **1** containing the conducting layer of the (BEDT-TTF)$_2$(I_xBr_{1-x})$_3$ nanocrystals.

with X-ray data and not contradictory to the presented thermodynamic consideration.

The quantitative analysis of the EPR signal of these BL-films, taking into account the EPR characteristics of both α′- and β-(BEDT-TTF)$_2$IBr$_2$ phases, is consistent with a very small (2−4%) amount of β-type nanocrystals in all the studied samples.

C. Structural Phase Transition at High Temperature. Taking into account that the well-known α′ → β (BEDT-TTF)$_2$IBr$_2$ phase transformation takes place at 156 °C,[18,19] we have looked for a similar structural phase transition for the new α′-(BEDT-TTF)$_2$(I_xBr_{1-x})$_3$ nanocrystals. To do so, we have studied the temperature dependence of the EPR signal of film **1** oriented perpendicular to the static magnetic field in a wide temperature region. As it was mentioned above, the EPR signal of the film samples consists of two different signals: one intensive but very broad signal of the α′-type nanocrystals with a line width (ΔH_{pp}) of 75 G and another small but narrower signal of the β phase impurity with ΔH_{pp} = 25 G. Since the observation of the temperature dependence of a broad signal is difficult, especially at high temperature, we have studied the temperature dependence of the narrow signal of the β phase impurity that has to increase during the α′ → β phase transition. The amplitude of the β phase signal was temperature independent up to 420 K (see Figure 2) and above 420 K the amplitude of the signal started to increase. A 8-fold buildup of the amplitude was observed about 440 K (Figure 2). Above 440 K the EPR signal with ΔH_{pp} = 25 G, g = 2.0070, which is characteristic of the β phases[7] (Scheme 2), becomes irreversibly dominant. This is an indication that the majority of the α′-(BEDT-TTF)$_2$(I_xBr_{1-x})$_3$ nanocrystals have been transformed to the metallic β_t-type nanocrystals.

To verify the orientation of the β_t-(BEDT-TTF)$_2$(I_xBr_{1-x})$_3$ nanocrystals which were formed during the third step, the EPR spectra of the annealed BL-film **1** in different orientations with respect to the static magnetic field were performed. The g factor variation is plotted in Figure 3. The g factor reaches a maximum when the magnetic field is perpendicular to the film plane and a minimum when it is parallel to that. This minimum g factor does not change upon rotation in the film plane. Since the maximum g value for the β-type single crystal[8] is found when the static magnetic field is parallel to the c* crystallographic axis, the above results allow us to conclude that the β_t-(BEDT-TTF)$_2$(I_xBr_{1-x})$_3$ nanocrystals are oriented with the c* axis perpendicular to the film plane. Thus, the EPR studies confirm the X-ray data (see below). In addition, the isotropic behavior found upon rotation around c* axis indicates that there is not a predominant in-plane orientation of the nanocrystals.

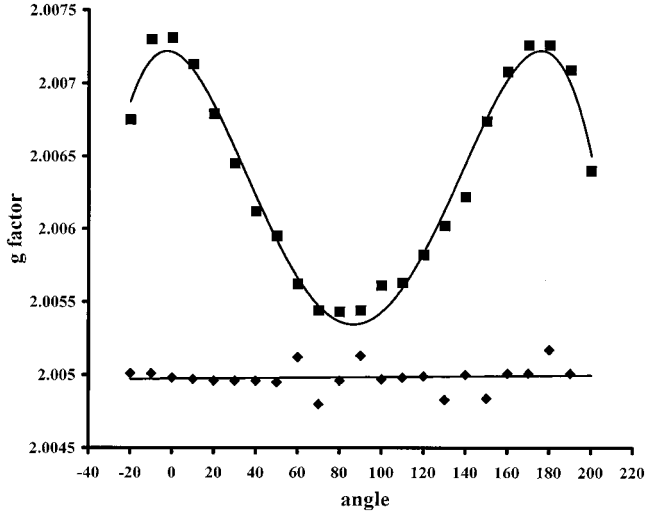

Figure 3. Angle dependence of g factor for film sample **1** containing the conducting layer of the β_t-(BEDT-TTF)$_2$(I_xBr_{1-x})$_3$ nanocrystals. (■) θ is the angle between the c* axis and the external magnetic field; (◆) rotation around the c* axis.

SCHEME 2: Schematic View of the α′ → β Structural Transformation of the BEDT-TTF Packing in the (BEDT-TTF)$_2$(I_xBr_{1-x})$_3$ Nanocrystals

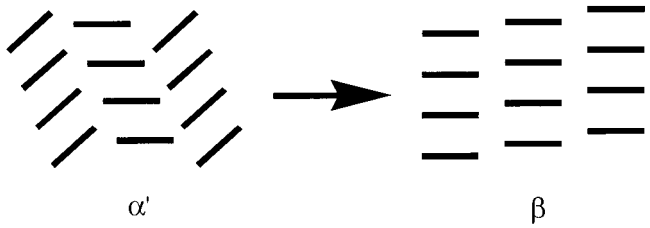

D. Composition and Structure of the BL-Film's Conducting Layers after Annealing. We have also tested all the film samples after 3 h annealing at 155−160 °C (Table 6) by X-ray

TABLE 6: Composition of the Conducting Layer of the BL-Film Samples after the Film Annealing

	X-ray data			
sample	d_{00l}, Å	phase	$(I_xBr_{1-x})_3$	conducting layer composition
1	15.038(3)	β	$x = 0.69(2)$	β-(BEDT-TTF)$_2$(I$_3$)$_y$(I$_2$Br)$_z$(IBr$_2$)$_{1-y-z}$[a]
2	15.04(1)	β	$x = 0.69(2)$	β-(BEDT-TTF)$_2$(I$_3$)$_y$(I$_2$Br)$_z$(IBr$_2$)$_{1-y-z}$
3	15.020(3)	β	$x = 0.61(3)$	β-(BEDT-TTF)$_2$(I$_3$)$_y$(I$_2$Br)$_z$(IBr$_2$)$_{1-y-z}$
4	15.01(1)	β	$x = 0.57(5)$	β-(BEDT-TTF)$_2$(I$_3$)$_y$(I$_2$Br)$_z$(IBr$_2$)$_{1-y-z}$
	16.33(1)	α'	$x = 0.33$	α'-(BEDT-TTF)$_2$IBr$_2$
	33.31(1)	new		N-salt
5	15.025(5)	β	$x = 0.63(3)$	β-(BEDT-TTF)$_2$(I$_3$)$_y$(I$_2$Br)$_z$(IBr$_2$)$_{1-y-z}$[a]
	15.013(3)	β	$x = 0.58(2)$	β-(BEDT-TTF)$_2$(I$_3$)$_y$(I$_2$Br)$_z$(IBr$_2$)$_{1-y-z}$
6	16.220(5)			BEDT-TTF
7	15.007(2)	β	$x = 0.55(2)$	β-(BEDT-TTF)$_2$(I$_3$)$_y$(I$_2$Br)$_z$(IBr$_2$)$_{1-y-z}$
8	16.31(1)	α'	$x = 0.33$	α'-(BEDT-TTF)$_2$IBr$_2$
	14.993(3)	β	$x = 0.50(2)$	β-(BEDT-TTF)$_2$ (I$_3$)$_y$(I$_2$Br)$_z$(IBr$_2$)$_{1-y-z}$
9	14.990(3)	β	$x = 0.44(2)$	β-(BEDT-TTF)$_2$(I$_3$)$_y$(I$_2$Br)$_z$(IBr$_2$)$_{1-y-z}$
	16.32(1)	α'	$x = 0.33$	α'-(BEDT-TTF)$_2$IBr$_2$
	33.32(1)	new		N-salt
10	14.995(5)	β	$x = 0.48(2)$	β-(BEDT-TTF)$_2$(I$_3$)$_y$(I$_2$Br)$_z$(IBr$_2$)$_{1-y-z}$
	16.32(1)	α'	$x = 0.33$	α'-(BEDT-TTF)$_2$IBr$_2$
	33.315(1)	new		N-salt

[a] The composition of the anion layer of these nanocrystals was found by Raman spectroscopy.

and Raman spectroscopies. In the X-ray diffraction patterns of annealed samples **1** and **5**−**7**, the reflections of the α'-(BEDT-TTF)$_2$(I$_x$Br$_{1-x}$)$_3$ phases ($0.66 > x \geq 0.33$) have disappeared. Instead, the strong reflections of a new phase arise. The d_{001} values of the reflections of annealed nanocrystals (Table 6) correspond to the β-type of the BEDT-TTF trihalide salts[8] (Scheme 2). In the case of β phases, based on the $d_{001}(x)$ composition dependence obtained from the known single-crystal cell parameters for β-(BEDT-TTF)$_2$I$_3$, β-(BEDT-TTF)$_2$I$_2$Br, and β-(BEDT-TTF)$_2$IBr$_2$, we were able to estimate the stoichiometry of the anion in the β-(BEDT-TTF)$_2$(I$_x$Br$_{1-x}$)$_3$ nanocrystals (Tables 4 and 6).

In the X-ray diffraction patterns of annealed samples **2** and **3** only intensive reflections of the β-(BEDT-TTF)$_2$(I$_x$Br$_{1-x}$)$_3$ salt with an x value of 0.70 and 0.61, respectively, are observed, and the reflections of the α'-type nanocrystals have disappeared. The X-ray diffraction patterns of annealed film samples **4** and **8**-**10** are more complicated. In the X-ray diffraction patterns of samples **4**, **9**, and **10** there are extra new reflections characteristic of the β-(BEDT-TTF)$_2$(I$_x$Br$_{1-x}$)$_3$ nanocrystals along with initial reflections of the α'-(BEDT-TTF)$_2$IBr$_2$ and N-salt. (Table 6). In the X-ray diffraction pattern of sample **8** the initial reflections of the α'-(BEDT-TTF)$_2$(I$_x$Br$_{1-x}$)$_3$ salt have disappeared. Instead, the 00l reflections of β-(BEDT-TTF)$_2$(I$_x$Br$_{1-x}$)$_3$ and α'-(BEDT-TTF)$_2$IBr$_2$ arise.

The presence of only 00l reflections of the β-type phases show that conducting layers generated during the third step consist of β_t–-type nanocrystals which are arranged just as those of the α'-type were aligned. Below let us focus on the d_{001} values corresponding to the β-type of the BEDT-TTF trihalide nanocrystals (Table 6). Experimentally, the d_{001} values of all β_t-type nanocrystals forming the conducting layer of the BL-films prepared are in the range from 14.990(3) Å to 15.04(1) Å. Since these d_{001} values are over the d_{001} value of the superconductor β-(BEDT-TTF)$_2$IBr$_2$ single crystal ($d_{001} = 14.95$ Å) and under the d_{001} value of the superconductor β-(BEDT-TTF)$_2$I$_3$ single crystal ($d_{001} = 15.109$ Å), we may conclude that, similarly to the α'-(BEDT-TTF)$_2$(I$_x$Br$_{1-x}$)$_3$ nanocrystals, the β_t-type nanocrystals contain the set of trihalide anions: IBr_2^-, I_3^-, and I_2Br^-. The X-ray data presented in Table 6 surprisingly show that at the third step of MRDT the stoichiometry of the anion layers of the (BEDT-TTF)$_2$(I$_x$Br$_{1-x}$)$_3$ nanocrystals has changed. This result is attributable to some solid-state reactions, which can take place during a BL-film annealing. For example, we have found that the decomposition of the conducting nanocrystals via reduction of BEDT-TTF$^{+\cdot}$ to a neutral molecule proceeds under the BL-films annealing (see experimental part). Therefore, it may be surmised that the $\alpha' \rightarrow \beta$ structural phase transition in the (BEDT-TTF)$_2$(I$_x$Br$_{1-x}$)$_3$ nanocrystals is probably accompanied by the following solid-state reactions:

$$\left.\begin{array}{l}\alpha'\text{-(BEDT-TTF)}_2(I_xBr_{1-x})_3\\ \beta\text{-(BEDT-TTF)}_2(I_xBr_{1-x})_3\\ \text{amorphous(BEDT-TTF)}/(I_xBr_{1-x})_3\end{array}\right\} \rightarrow \text{BEDT-TTF} + \text{IBr} \rightleftharpoons \begin{cases}\alpha'_t\text{-(BEDT-TTF)}_2\text{IBr}_2\\ \beta_t\text{-(BEDT-TTF)}_2(I_xBr_{1-x})_3 \text{ mainly}\\ \text{amorphous}_t\ \text{(BEDT-TTF)}/(I_xBr_{1-x})_3\end{cases}$$

In accordance with thermodynamic consideration:

$$I(\alpha'+\beta+\text{amorphous}):Br(\alpha'+\beta+\text{amorphous}) = 1:1$$
$$I(\alpha'_t+\beta_t+\text{amorphous}_t):Br(\alpha'_t+\beta_t+\text{amorphous}_t) = 1:1$$

In that case, the $x(\alpha')$, $x(\alpha'_t)$, and $x(\beta_t)$ values can be different. Previously, we also observed the decomposition of the (BEDT-TTF)$_2$I$_3$ nanocrystals under the film annealing during the MRDT third step. To prevent the loss of iodine and decomposition of the nanocrystals at the $\alpha \rightarrow \beta_t$ (BEDT-TTF)$_2$I$_3$ transition, we have annealed these BL-film samples in the presence of a small amount of I$_2$ vapors.

The same solid-state reactions can also accompany the $\alpha \rightarrow \beta$ and $\alpha' \rightarrow \beta$ transitions in the single crystals of the BEDT-TTF trihalide salts, but for those the loss of halogen in a remarkable amount was not observed.[9,18,19] It seems plausible that these speculative solid-state reactions proceeding in the surface layer of a solid are of a little importance for bulk single crystals but they can be crucial for the delicate BL-film's nanocrystals with a rich developed surface.

According to the Raman spectrum of sample **1,** the β_t-(BEDT-TTF)$_2$(I$_x$Br$_{1-x}$)$_3$ nanocrystals contain the set of bands due to the vibrations of thihalide anions such as I_3^- (121 cm^{-1}), I_2Br^- (140 cm^{-1}), and IBr_2^- (167 cm^{-1}). Unfortunately, the low-frequency Raman spectra of the other annealed BL-film samples were poor due to a luminescence appearing in the BL-films annealed. The reason for that is not clear.

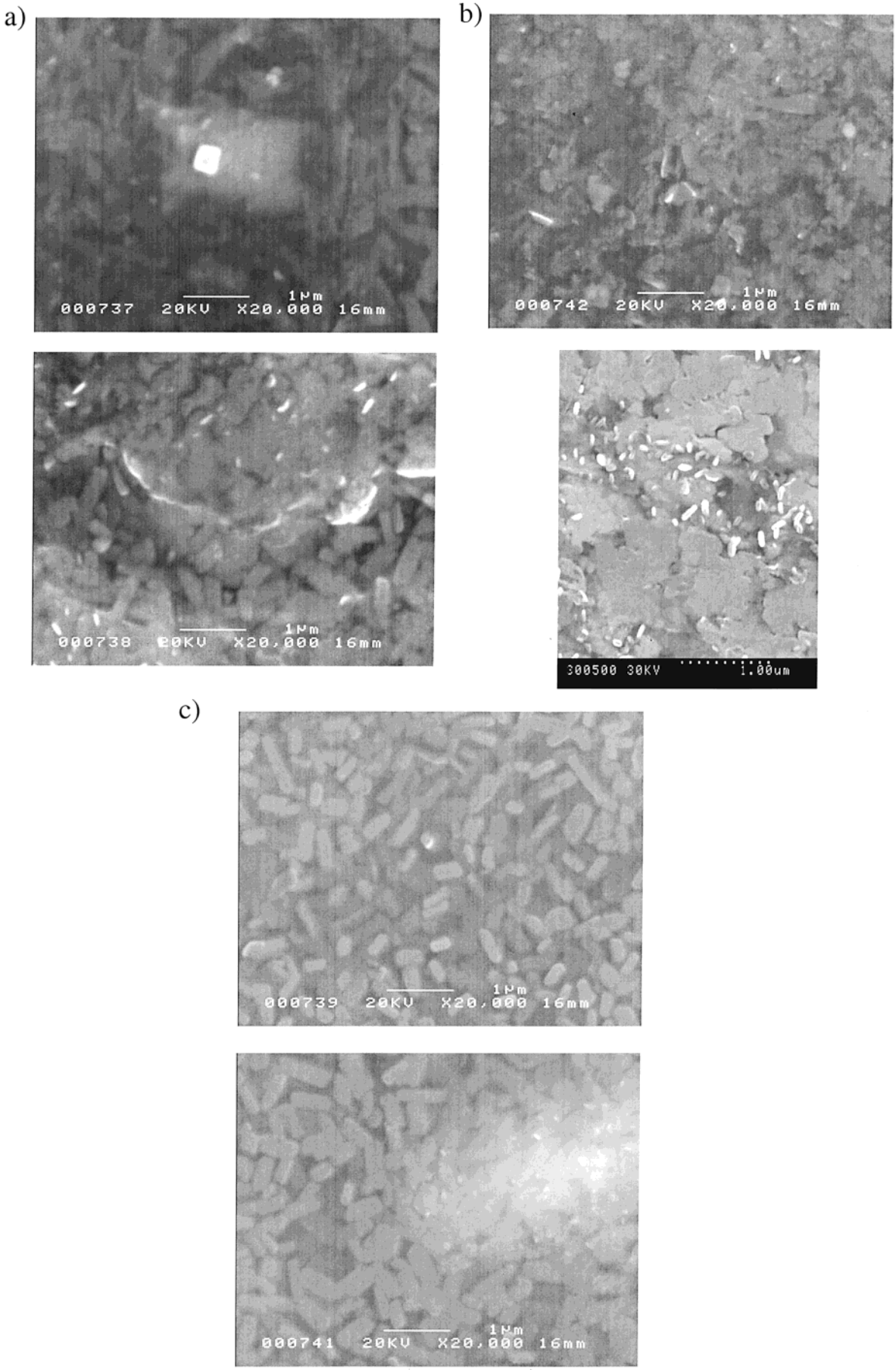

Figure 4. SEM images of BL-film samples (a) **1**, (b) **7**, and (c) **8** after the second (top) and third steps (bottom) of MRDT.

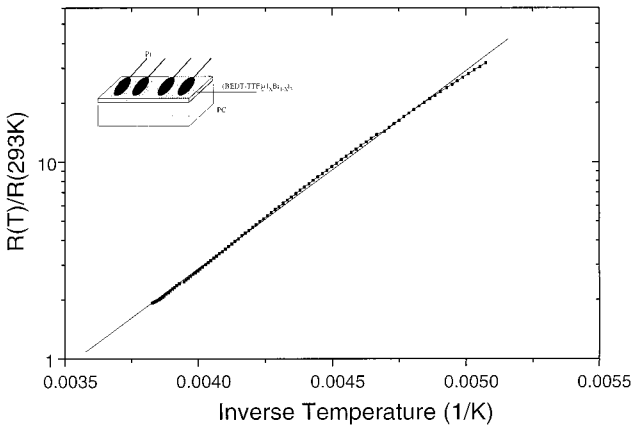

Figure 5. Normalized resistance of the conducting surface layer of the α′-(BEDT-TTF)$_2$(I_xBr_{1-x})$_3$ nanocrystals versus inverse temperature (sample **1** after the second step of MRDT). Inset shows the geometry of electrical contacts in a BL-film sample.

E. Textures of the Conducting Layers: SEM Studies. Taking into account that the quality of the nanocrystalline surface layer is very important in order to impart the electrical properties of molecular metals to the BL-films, we have studied the morphology (size, shape and orientation) of the (BEDT-TTF)$_2$(I_xBr_{1-x})$_3$ nanocrystals formed during the second and third step of MRDT. We have obtained the SEM images of samples **1**, **7**, and **8** (Figure 4). These samples were chosen as the typical BL-films containing the conducting surface layer of α′-(BEDT-TTF)$_2$(I_xBr_{1-x})$_3$ nanocrystals. According to the SEM images, all film samples contain a well oriented conducting layer: the largest faces of nanocrystals are parallel to the film surface. The texture of the α′-type conducting layer of sample **1** formed at the lowest F_{IBr} value consists of very small and poorly shaped nanocrystals (Figure 4a, top). By contrast, the nanocrystals of sample **8** are bigger and better shaped (Figure 4c, top). The textures of BL-films after annealing are shown in the bottom of Figure 4. The comparative analysis of these SEM images indicate that the textures of BL-films before and after annealing differ considerably: the β-type nanocrystals are better shaped and bigger than those of the initial α′-type nanocrystals.

F. Electrical Properties. To study the transport properties, rectangular pieces (≅1.5 × 0.5 mm^2) were cut out from the BL-film samples. The temperature dependence of the resistance of the BL-film samples was measured down to helium temperature. The typical temperature dependence of normalized resistance of the α′- and β_t-conducting layers is depicted in Figures 5 and 6, respectively. The resistance of the α′-conducting layers increases very strongly in decreasing temperature (Figure 5). When the temperature decreases from 300 to 175 K the resistance of the samples increases by a factor 100 with the activation energy value being equal to 0.2 eV, which is identical to that for the α′-(BEDT-TTF)$_2$IBr$_2$ single crystal. In contrast, the temperature dependence of resistance of the β_t-type conducting layers (samples **1**, **2**, and **5**−**7)** is metal-like down to nitrogen temperature, but at lower temperatures resistance starts to increase slightly. For example, the temperature dependence of resistance of sample **1** is presented in Figure 6 (curve a). The *R*(*T*) behavior of the annealed conducting layers which contain the β_t-(BEDT)$_2$(I_xBr_{1-x})$_3$ nanocrystals along with those of the α′-(BEDT-TTF)$_2$IBr$_2$ phase and N-salt is not metal-like: it increases with decreasing temperature (Figure 6, curve b), but all these samples are conductors down to helium temperature. Since the known β-type single crystals of BEDT-TTF with mixed trihalide anion[13] are

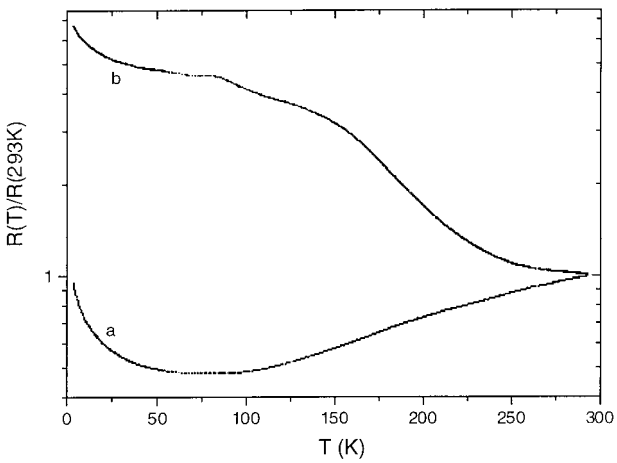

Figure 6. Typical temperature dependence of normalized resistance for different conducting surface layers containing the β_t-(BEDT-TTF)$_2$(I_xBr_{1-x})$_3$ nanocrystals as a main component: (a) film sample **1** and (b) film sample **8** (see text, Table 6).

metallic down to 1.5 K, we have expected that all the β_t-(BEDT-TTF)$_2$(I_xBr_{1-x})$_3$ conducting layers would show also the metal-like behavior of resistance down to helium temperature. However, the resistance of the β_t-type conducting layers of samples **1**, **2**, or **5**−**7** is not metal-like below nitrogen temperature. The transport properties of conducting layers in general depend on the conducting properties of the nanocrystals forming the layer as well as on the quality and the number of contacts between them. According to X-ray and SEM data the β_t-(BEDT-TTF)$_2$(I_xBr_{1-x})$_3$ nanocrystals are well "*c**" oriented and developed. Thus, one may conclude that the quality and/or number of contacts are not sufficient to form a continuous conducting layer revealing metal-like transport properties down to helium temperature.

4. Summary

A set of new conducting BL-films consisting of the polymeric PC/BEDT-TTF layer and thin surface layer of oriented (BEDT-TTF)$_2$(I_xBr_{1-x})$_3$ nanocrystals was prepared. All new transparent, flexible, and lightweight BL-films are conductors in a wide temperature region and some of them reveal metallic transport properties down to 80 K.

In the context of a thermodynamic approach, it was shown for the first time that the reduction of IBr should result in the formation of I_3^-, I_2Br^-, and IBr_2^- anions, giving the IBr_2^- species the major contribution. Ab initio calculations indicate that the contribution of these anions can depend on the polarity of the environment.

It was also shown that the α′ → β structural phase transition in the (BEDT-TTF)$_2$(I_xBr_{1-x})$_3$ nanocrystals takes place around 160−170 °C.

Acknowledgment. We are grateful to Dr. V. Laukhin and Prof. R. P. Shibaeva for useful discussions as well as to Dr. L. Buravov for help with dc-conductivity measurements.This work was supported by NATO (Project CRG.LG.974316), by DGI−Spain (BQU2000-1157), by Generalitat de Catalunya (2000 SGR-00114), by the Russian Foundation for Basic Research (Project 00-03-33200), by the Russian National Program "*Physics of Quantum and Wave Processes*", and by Polish State Committee for Scientific Research, Grant 7T08E06614p02. E.L. is grateful to Spanish Ministerio de Educacion y Cultura for Sabbatical at ICMAB (CSIC).

References and Notes

(1) Laukhina, E. E.; Merzhanov, V. A.; Pesotskii, S. I.; Khomenko, A. G.; Yagubskii, E. B.; Ulanski, J.; Kryszewski, M.; Jeszka, J. K. *Synth. Met*. **1995**, *70*, 797.

(2) Ulanski, J.; Kryszewski, M. In *The Encyclopedia of Advanced Materials*; Bloor, D., Brook, R. J., Fleming, M. C., Mahajan, S., Cahn, R. W., Eds.; Pergamon: Oxford, 1994; p 2301.

(3) Laukhina, E.; Tkacheva, V.; Shibaeva, R.; Khasanov, S.; Rovira, C.; Veciana, J.; Vidal-Gancedo, J.; Tracz, A.; Jeszka, J. K.; Sroczynska, A.; Wojciechowski, R.; Ulanski, J.; Laukhin, V. *Synth. Met.* **1999**, *102*, 1785.

(4) Jeszka, J. K.; Tracz, A. *Polym. Adv. Technol.* **1992**, *3*, 139.

(5) Williams, J. M.; Ferraro, J. R.; Thorn, R. J.; Carlson, K. D.; Geiser, U.; Wang, H. H.; Kini, A. M.; Whangbo, M.-H. *Organic Superconductors (Including Fullerenes): Synthesis, Structure, Properties, and Theory*; Prentice Hall: Englewood Cliffs, New Jersey, 1992.

(6) Horiuchi, S.; Yamochi, H.; Saito, G.; Jeszka, J. K.; Tracz, A.; Sroczyñska, A.; Ulanski, J. *Mol. Cryst. Liq. Cryst.* **1997**, *296*, 365.

(7) Ulanski, J.; Tracz, A.; Jeszka, J. K.; Laukhina, E.; Khomenko, A.; Polanowski, P.; Staerk, D.; Helberg, H. W. In *NATO ARW: Electrical and Related Properties of Organic Solids*; Munn, R. W., Kuchta, B., Miniewich, A., Ed.; Kluwer: Dordrecht, 1996; p 241.

(8) Laukhina, E. E.; Ulanski, J.; Khomenko, A. G.; Pesotskii, S. I.; Tkachev, V.; Atovmyan, L.; Yagubskii, E. B.; Rovira, C.; Veciana, J.; Vidal-Gancedo, J.; Laukhin, V. *J. Phys. I Fr.* **1997**, *7*, 1665.

(9) Baran, G. O.; Buravov, L. I.; Degtyarev, L. S.; Kozlov, M. E.; Laukhin, V. N.; Laukhina, E. E.; Onishchenko, V. G.; Pokhodnya, K. I.; Sheinkman, M. K.; Shibaeva, R. P.; Yagubskii, E. B. *Pis'ma Zh. Eksp. Teor. Fiz.* (USSR) **1986**, 44, 6, 293; *JETP Lett.* (U.S.A.) **1986**, *44*, 376 (English translation).

(10) Creuzet, F.; Creuzet, G.; Jerome, D.; Schweitzer, D.; Keller, H. J. *J. Phys. Lett.* **1985**, *46*, 1079.

(11) Frisch, M. J.; Trucks, G. W.; Schlegel, H. B.; Gill, P. M. W.; Johnson, B. G.; Robb, M. A.; Cheeseman, J. R.; Keith, T. A.; Peterson, G. A.; Montgomery, J. A.; Raghavachari, K.; Al-Laham, M. A.; Zakrzewski, V. G.; Ortiz, J. V.; Foresmen, J. B.; Peng, C. Y.; Ayala, P. Y.; Wong, M. W.; Andres, J. L.; Replogle, E. S.; Gomperts, R.; Martin, R. L.; Fox, D. J.; Binkley, J. S.; Defrees, D. J.; Baker, J.; Stewart, J. P.; Head-Gordon, M.; Gonzalez, C.; Pople, J. A. *Gaussian 94*, revision D.1; Gaussian, Inc.: Pittsburgh, PA, 1995.

(12) Wong, M. W.; Wiberg, K. B.; Frisch, M. J. *J. Am. Chem. Soc.* **1992**, *114*, 523.

(13) Laukhina, E. E.; Narymbetov, B. Zh.; Zorina, L. V.; Khasanov, S. S.; Rozenberg, L. P.; Shibaeva, R. P.; Buravov, L. I.; Yagubskii, E. B.; Avramenko, N. V.; Van, K. *Synth. Met.* **1997**, *90*, 101.

(14) Wojciechowski, R.; Ulanski, J.; Lefrant, S.; Faulques, E.; Laukhina, E.; Tkacheva, V. *J. Chem. Phys.* **2000**, *112*, 7634.

(15) Atkins, P. W. *Physical Chemistry*; Oxford University Press: New York, 1978.

(16) Shibaeva, R. P.; Kaminskii, V. F.; Linderman, S. V.; Yagubskii; E. B. *Sov. Phys. Crystallogr.* **1986**, *31*, 546 (English Translation).

(17) Sugai, S.; Saito, G. *Solid State Commun.* **1986**, *58*, 759.

(18) Avramenko, N. V.; Zvarykina, A. V.; Laukhin, V. N.; Laukhina, E. E.; Lubovskii, R. B.; Shibaeva,R. P. *JETP Lett.* **1988**, *48*, 472.

(19) Wang, H. H.; Carson, K. D.; Montgomery, L. K.; Schlueter, J. A.; Cariss, C. S.; Kwok, W. K.; Geiser, U.; Crabtree, G. W.; Williams, J. M. *Solid State Commun.* **1988**, *66*, 1113.

ARTICLE E

Títol: New transparent metal-like bi-layer composite films with high conducting layers of the θ-(BET-TTF)$_2$Br·3H$_2$O nanocrystals.

Autors: M. Mas–Torrent, E. Laukhina, C. Rovira, J. Veciana, V. Tkacheva, L. Zorina and S. Khasanov.

Publicació: *Adv. Funct. Mater.*, 11, 4, 299-303.

Any: 2001

New Transparent Metal-like Bilayer Composite Films with Highly Conducting Layers of θ-(BET-TTF)$_2$Br·3H$_2$O Nanocrystals**

By *Marta Mas-Torrent*, *Elena Laukhina*,* *Concepció Rovira*,* *Jaume Veciana*, *Vladislava Tkacheva*, *Leokadiya Zorina*, and *Salavat Khasanov*

A flexible low-density metallic material, which is extremely transparent, was obtained using as active component the highly conducting molecular metal θ-(BET-TTF)$_2$Br·3H$_2$O, BET-TTF = bis(ethylenethio)tetrathiafulvalene. This material is a bilayer (BL) film that was prepared by treating a polycarbonate film containing 2 wt.-% of molecularly dispersed BET-TTF with vapor of a Br$_2$/CH$_2$Cl$_2$ solution. Optimum conditions for the preparation of very transparent metallic materials were established. The X-ray diffraction patterns indicate that the conducting layer of the BL films is formed by well *a** oriented θ-(BET-TTF)$_2$Br·3H$_2$O nanocrystals, which are clearly observed in the SEM images. Conductivity measurements confirm that the nanocrystalline layers have the same transport properties as those of the single crystals, displaying metal-like behavior down to He temperature and the highest room temperature conductivity (120 Ω^{-1} cm^{-1}) reported so far for this kind of film.

1. Introduction

The layered structure and exceptionally high room temperature conductivity (350–3900 Ω^{-1} cm) of the novel θ-(BET-TTF)$_2$Br·3H$_2$O [BET-TTF: bis(ethylenethio)tetrathiafulvalene] molecular metal[1] make it very attractive as the base component for the conducting layer of bilayer (BL) composite films, which consist of a polycarbonate matrix with a conducting surface layer formed of a crystalline network of organic conductors.[2–5] Moreover, the hint of a superconducting transition observed in some θ-(BET-TTF)$_2$Br·3H$_2$O crystals[1] has also encouraged the use of this compound in these composite materials. BL films permit the high stability and different physical properties of crystalline organic conductors[6] to be combined with the advantageous properties of polymeric matrices such as flexibility, transparency, and low density. Furthermore, BL films can be produced with different sizes and shapes, which could be of technical interest. Therefore, they have clear advantages compared with single crystals of molecular conductors with respect to potential applications in a new generation of electronic devices. The few known BL films were prepared by a modified reticulate doping technique (MRDT),[2,3,7] which involves the generation of a conducting layer via a D (donor) + Hal (halogen) reaction.[2–5] For example, conducting layers consisting of α-(BEDT-TTF)$_2$I$_3$ and (BEDO-TTF)$_2$Br·3H$_2$O nanocrystals were formed by the reactions BEDT-TTF + I$_2$[2] and BEDO-TTF + Br$_2$,[4] respectively [BEDT-TTF: bis(ethylenedithio)tetrathiafulvalene; BEDO-TTF: bis(ethylenedioxo)-tetrathiafulvalene]. The latter result gives grounds to expect the formation of a surface conducting layer of θ-(BET-TTF)$_2$Br·3H$_2$O nanocrystals from the BET-TTF + Br$_2$ reaction, although the initial single crystals of the salt were synthesized by an electrochemical method.[1] So, in order to generate a conducting layer of θ-(BET-TTF)$_2$Br·3H$_2$O nanocrystals we applied the same MRDT procedure as used in the preparation of the known BL conducting films[2–5] but using BET-TTF in the first step and bromine in the second step of the MRDT (Fig. 1). This methodology has enabled us to produce a new, very transparent BL film with metal-like behavior of the resistance down to liquid helium temperature and the highest room temperature conductivity of any BL film reported to date.

2. Results and Discussion

Polycarbonate (PC) films with a typical thickness of 10–15 μm containing 2 wt.-% of molecularly dispersed BET-TTF were cast as previously described.[2,7] Then the surfaces of the samples were treated with the vapor of a Br$_2$/CH$_2$Cl$_2$ solution, producing the BET-TTF + Br$_2$ reaction in the swollen film surface (Fig. 1). The ratio of the reagents employed during the reaction is very important because it determines whether a completely ionic non-conducting salt is formed and/or a mixed

[*] Dr. E. Laukhina,[+] Dr. C. Rovira, M. Mas-Torrent, Prof. J. Veciana
Institut de Ciència de Materials de Barcelona (CSIC)
Campus Universitari de Bellaterra, E-08193 Cerdanyola (Spain)
E-mail: c.rovira@icmab.es

V. Tkacheva
Institute of Problems of Chemical Physics, RAS
Chernogolovka, MD 142432 (Russia)

L. Zorina, Dr. S. Khasanov
Institute of Solid State Physics, RAS
Chernogolovka, MD 142432 (Russia)

[+] Permanent address: Institute of Problems of Chemical Physics, RAS, Chernogolovka, MD 142432, Russia. E-mail: liv@icp.ac.ru.

[**] This work was supported by NATO (project No CRG.LG.974316), by DGI-Spain (BQU2000–1157), by the Generalitat de Catalunya (2000 SGR-00114), and by the Russian Foundation for Basic Research (Project No. 00-03–33200). We are grateful to Dr. R. Shibaeva for useful discussions, EL is grateful to the Spanish Ministerio de Educacion y Cultura for a Sabbatical Fellowship at ICMAB (CSIC), and MMT is grateful to the Generalitat de Catalunya for a predoctoral grant.

  1616-301X/01/0408-0299 $ 17.50+.50/0

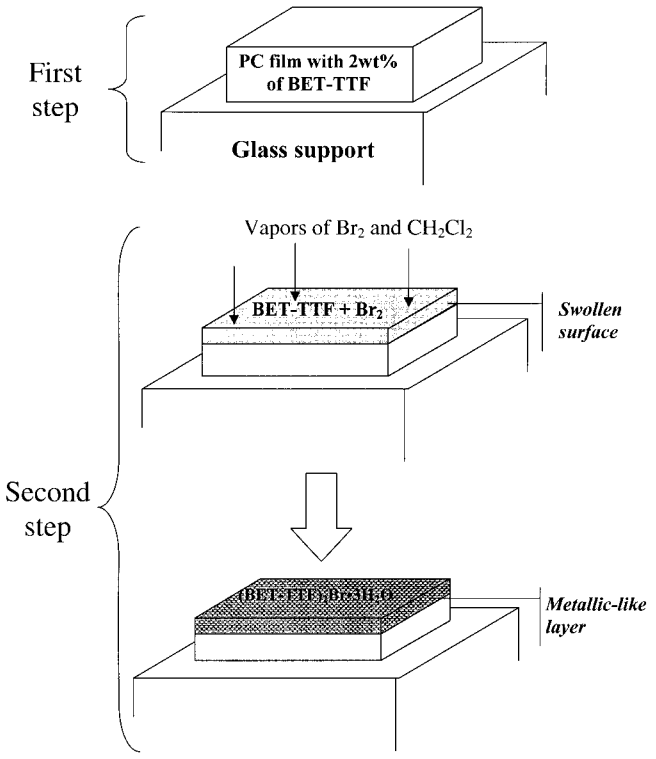

Fig. 1. Scheme of the preparation by MRDT of the new BL film with a conducting surface layer of θ-(BET-TTF)$_2$Br·3H$_2$O nanocrystals.

valence metallic salt. We suggest that an optimum mass of Br_2 absorbed per unit volume of a swollen film surface layer ($C_{Br/film}$) exists, at which a conducting layer of θ-(BET)$_2$Br·3H$_2$O nanocrystals is achieved. Generally, the $C_{Br/film}$ value is proportional to: i) the mass of Br_2 in the vapor of the Br_2/CH_2Cl_2 solution ($m_{Br/v}$), and ii) the duration of the film surface treatment (t). According to the gas state equations[8] and Henry's law,[8] the value of $m_{Br/v}$ is proportional to the mole fraction of Br_2 (x_{Br}*) contained in the Br_2/CH_2Cl_2 solution, and it can be shown that

$$C_{Br/film} \approx D_{Br} C_{Br/s} V_s t \quad (1)$$

where D_{Br} is the capability of Br_2 vapor to penetrate into a swollen polycarbonate layer, $C_{Br/s}$ is the molar concentration of Br_2 in the Br_2/CH_2Cl_2 solution, and V_s is the volume of this solution. In order to find the optimum value of $C_{Br/film}$ we prepared film samples 1–7 using different $C_{Br/s}$ and t values (see Table 1). In all experiments the amount of BET-TTF, the treated film surface area (7 cm^2), and the volumes of vapor (29.5 mL) and solution (10.5 mL) were identical. The second steps were carried out at the same temperature to fix the following parameters: D_{Br}, rate of reaction, and rate of reagent diffusion. Taking into account the outlined peculiarities of the second step of the MRDT, we may restrict ourselves to the simple estimation of the $C_{Br/film}$ values with respect to the factor F_{Br}, which is proportional to the molar concentration of Br_2 in CH_2Cl_2 and the duration of the film surface treatment (Table 1):

$$F_{Br} = C_{Br/s} t \quad (2)$$

Table 1. Parameters of the second step of MRDT: ambient temperature (T), molar concentration of Br_2 in CH_2Cl_2 ($C_{Br/s}$), duration of the treatment (t), and value of the factor F_{Br}.

Film sample	T [°C]	$C_{Br/s}$ [M]	Treatment duration [min]	F_{Br} [10^{-2} M min]
1	22	2×10^{1}	1	20
2	22	1×10^{-1}	1	10
3	22	4×10^{-3}	6	2.4
4	24	4×10^{-3}	4	1.6
5	24	4×10^{-3}	2	0.8
6	24	4×10^{-3}	1.5	0.6
7	24	4×10^{-3}	0.5	0.2

It is important to note that samples 3–7, produced at $F_{Br} \leq 2.4 \times 10^{-2}$ M min, are very slightly orange colored and extremely transparent, while all samples produced at higher F_{Br} values are green and more opaque. Figure 2 demonstrates how sample 6, which has metal-like transport properties down to liquid He temperature and an exceptionally high σ_{293K} value for BL films (Fig. 3b, Table 2), is completely transparent.

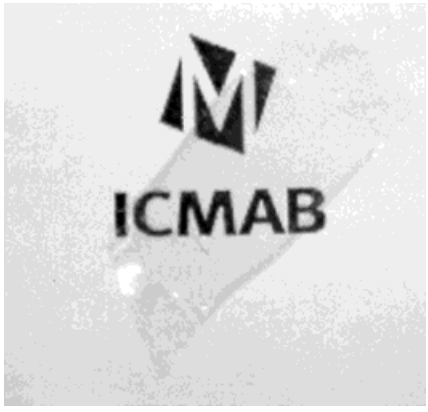

Fig. 2. View through the new metal-like BL film with a surface layer of θ-(BET-TTF)$_2$Br·3H$_2$O nanocrystals (sample 6).

The electrical properties of the new film samples were studied and the σ_{293K} value calculated. For this purpose rectangular pieces (~1.5 mm × 0.5 mm) were cut out of the BL film samples. The resistance of samples was measured by a standard four-probe DC method: four annealed platinum wires (20 μm in diameter) were attached to the treated surface of a BL film by a conductive graphite paste (see inset to Fig. 3b). In agreement with DC measurements (Table 2), only film samples that were produced at low F_{Br} values possessed a conducting layer. The σ_{293K} values of samples 5 and 6 (120 and 95 Ω^{-1}cm^{-1}, respectively) are extremely high compared with known BL films.[2–5] The temperature dependence of the resistance of film samples 4–6 was measured down to 4 K (Table 2). According to DC data presented in Figure 3a, sample 4 has metallic transport properties in a wide temperature range (250–20 K). Samples 5 and 6 demonstrate metal-like transport properties down to liquid He temperature (Fig. 3b). The temperature dependence of the normalized resistance of conducting BL films 3 and 7 was not measured since both samples have a very low value of conductivity at room temperature (Table 2). There-

  1616-301X/01/0408-0300 $ 17.50+.50/0

ADVANCED FUNCTIONAL MATERIALS

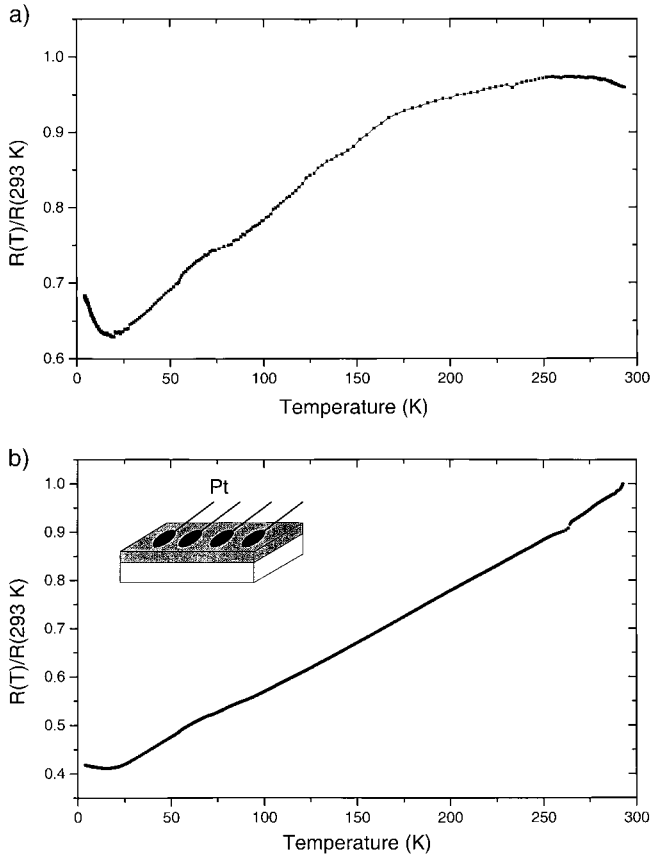

Fig. 3. Normalized resistance of the conducting surface layer of θ-(BET-TTF)$_2$Br·3H$_2$O nanocrystals versus temperature: a) sample 4; b) sample 6; the inset shows the geometry of electrical contacts to the film sample.

Table 2. Electrical properties and X-ray data (composition) of the BL film surface layers after the second MRDT step.

Film sample	Electrical properties		X-ray data	
	σ_{293K} [Ω^{-1}cm^{-1}]	Type of surface layer	d_{100} [Å]	Composition
1	$> 10^{-5}$	Dielectric	Amorphous	–
2	$> 10^{-5}$	Dielectric	Amorphous	–
3	0.017	Conducting	15.285(5)	θ-(BET-TTF)$_2$Br·3H$_2$O and another phase of (BET-TTF)Br$_x$ [a]
4	21	Metallic in the range 250–20 K	15.315(5)	θ-(BET-TTF)$_2$Br·3H$_2$O
5	120	Metallic down to 4 K	15.37(5)	θ-(BET-TTF)$_2$Br·3H$_2$O
6	95	Metallic down to 4 K	15.325(5)	θ-(BET-TTF)$_2$Br·3H$_2$O
7	0.04	Conducting	15.30(1)	θ-(BET-TTF)$_2$Br·3H$_2$O

[a] In line with NIR spectra and SEM data (see text).

fore, the analysis of conductivity data shows that the values of F_{Br} in the range 0.016–0.006 M min provide the optimum $C_{Br/film}$ value, which allows the generation of a metal-like conducting layer in these new BL films.

As it has previously been shown that the measured values of the interplanar spacing d_{001} along with intensities of (00l) reflections allow the identification of the different phases of the BEDT-TTF trihalides,[3] we studied the X-ray diffraction patterns of conducting samples 3–7 in order to clarify which kind of nanocrystal forms the conducting layer of the new BL film samples (Table 2). The X-ray diffraction patterns[9] of all the samples (Fig. 4 shows sample 5) indicate the presence of only (h00) reflections, which are characteristic of conducting layers

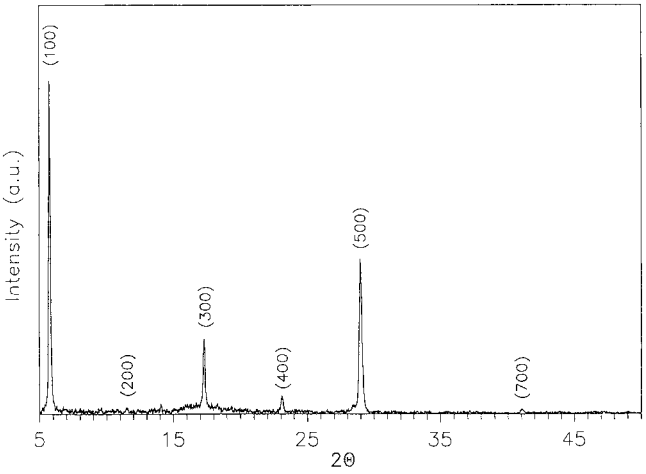

Fig. 4. X-ray diffraction pattern of sample 5.

formed by oriented nanocrystals: the crystallographic a*-axis of nanocrystals is perpendicular and consequently their conducting layers are parallel to the film surface.[3] The measured values of the interplanar spacing d_{100} and the relative intensity of the lines of the nanocrystals for all the samples correspond to the θ-(BET-TTF)$_2$Br·3H$_2$O phase (d_{100} = 15.24(1) Å).[1] It is important to note that the reflections of the θ-(BET-TTF)$_2$Br·3H$_2$O phase in the X-ray diffraction patterns of samples 3 and 7 are much weaker than those in the X-ray diffraction patterns of metal-like samples 5 and 6. These X-ray results indicate that the novel metal-like surface layer of the θ-(BET-TTF)$_2$Br·3H$_2$O nanocrystals can be generated by the BET-TTF + Br$_2$ reaction.

The near-infrared (NIR) spectra of all conducting BL films were measured.[10] The NIR spectra of samples 4–7 (Fig. 5, top) are practically identical, containing two bands: a band at 830 nm (B band) and a very wide band centered at 4300 nm (A band), which are typical of TTF-derivative mixed valence salts.[11] It is worth noting that these spectra are very similar to that of θ-(BET-TTF)$_2$Br·3H$_2$O single crystals,[1] in good agreement with the X-ray data. In the spectrum of sample 3 a new intense extra band appears at 1550 nm and the B band becomes stronger (Fig. 5, bottom). In accordance with these results, we can surmise that the conducting layer of sample 3 mainly contains another amorphous BET-TTF salt (A), which should have ionic character.

Thus, we are able to assume that the formation of salt A in a significant amount results in the very low σ_{293K} value of sample 3 (Table 2). In contrast, the low σ_{293K} value of sample 7 (σ_{293K} = 0.04 Ω^{-1}cm^{-1}) could be due to the poorly developed polycrystalline layer of θ-(BET-TTF)$_2$Br·3H$_2$O nanocrystals, which was produced at the lowest F_{Br} and $C_{Br/film}$ values and as a consequence grew poorly.

  1616-301X/01/0408-0301 $ 17.50+.50/0

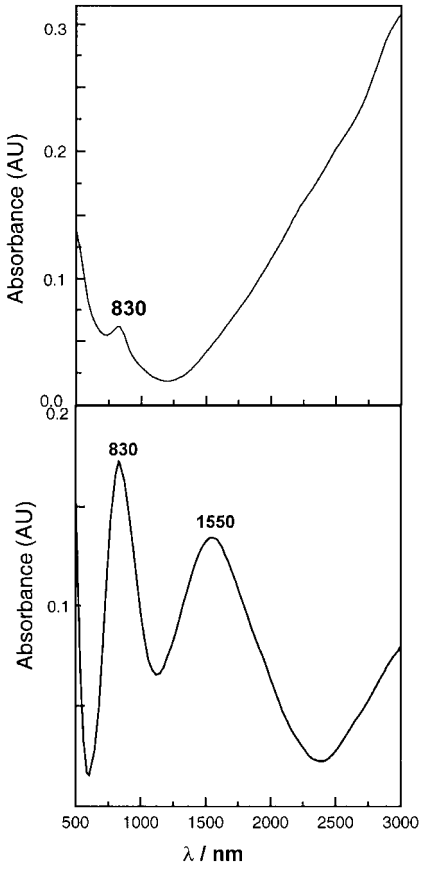

Fig. 5. NIR spectra of the conducting surface layer of θ-(BET-TTF)$_2$Br·3H$_2$O nanocrystals: sample 6 (top) and sample 3 (bottom).

Taking into account that the quality of linked nanocrystals is very important in order to impart the electrical properties of the single crystals of a molecular metal to the conducting layer of BL films, we have studied the texture of BL films with conducting layers of θ-(BET-TTF)$_2$Br·3H$_2$O nanocrystals.[12] Scanning electron microscopy (SEM) images of samples 4, 6, and 7 are presented in Figure 6. For comparison we also present a typical SEM image of a dielectric "green" sample prepared at an F_{Br} value greater than 0.03 M min (sample 1, Fig. 6d). As was expected, in the SEM image of sample 7 poorly developed nanocrystals can be observed (Fig. 6a). For samples 5 and 6, which have the most interesting electrical properties (see Table 2), SEM images showing very well shaped nanocrystals were obtained (Fig. 6b). Regarding the well-formed shape of the nanocrystals, we can see that they have angles that are characteristic of θ-type single crystals, in agreement with X-ray and NIR data. These nanocrystals are oriented, their largest faces (which correspond to the *bc* conducting planes) being parallel to the film surface, and they completely cover the surface of the sample, forming a layer. In the SEM image of sample 6 a few non-conducting needles are also observed, which can be attributed to some nanocrystals of non-reacted BET-TTF. In the SEM image of sample 4 (Fig. 6c) quite good nanocrystals are also observed, although they are not so highly developed as in samples 5 and 6. Furthermore, some bright crystallites and amorphous globules can be seen, which show the presence of another non-conducting phase. The bright amorphous globules become dominant in the SEM images of all dielectric "green" BL films (Fig. 6d). These results indicate that the formation of the non-conducting amorphous layer of a BET-TTF salt with the Br^- anion by the BET-TTF + Br_2 reaction takes place at F_{Br} values higher than 0.03 M min.

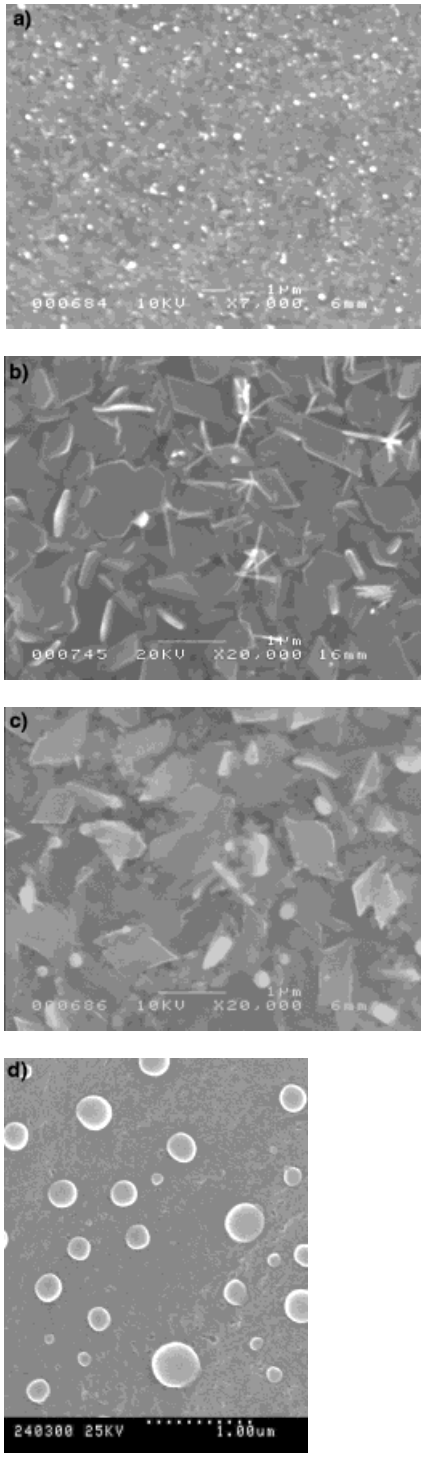

Fig. 6. SEM images of the surface layer of BL films: a) sample 7, b) sample 6, c) sample 4, d) sample 1.

  1616-301X/01/0408-0302 $ 17.50+.50/0

ADVANCED FUNCTIONAL MATERIALS

3. Conclusions

We have developed a new conducting bilayer composite film with the surface layer formed by θ-(BET-TTF)$_2$Br·3H$_2$O nanocrystals. This flexible low-density material, which is extremely transparent, has metal-like transport properties down to liquid helium temperature along with a very high value of conductivity at room temperature similar to that of single crystals of organic conductors. Optimum conditions for BL film preparation ($C_{Br/s}$ and t) were established, which provide the optimum ratio of reagents during the BEDT-TTF + Br_2 reaction in order to generate a metal-like layer of highly oriented and well-connected θ-(BET-TTF)$_2$Br·3H$_2$O nanocrystals. The development of transparent highly conducting films opens up new avenues for the possible application of organic metals.

Received: April 3, 2001

[1] E. Laukhina, E. Ribera, J. Vidal-Gancedo, S. Khasanov, L. Zorina, R. Shibaeva, E. Canadell, V. Laukhin, M. Honold, M.-S. Nam, J. Singleton, J. Veciana, C. Rovira, *Adv. Mater.* **2000**, *12*, 54.

[2] E. E. Laukhina, V. A. Merzhanov, S. I. Pesotskii, A. G. Khomenko, E. B. Yagubskii, J. Ulanski, M. Kryszewski, J. K. Jeszka, *Synth. Met.* **1995**, *70*, 797.

[3] E. E. Laukhina, J. Ulanski, A. G. Khomenko, S. I. Pesotskii, V. Tkachev, L. Atovmyan, E. B. Yagubskii, C. Rovira, J. Veciana, J. Vidal-Gancedo, V. Laukhin, *J. Phys. I* **1997**, *7*, 1665.

[4] S. Horiuchi, H. Yamochi, G. Saito, J. K. Jeszka, A. Tracz, A. Srocyñska, J. Ulanski, *Mol. Cryst. Liq. Cryst.* **1997**, *296*, 365.

[5] E. Laukhina, V. Tkacheva, R. Shibaeva, S. Khasanov, C. Rovira, J. Veciana, J. Vidal-Gancedo, A. Tracz, J. K. Jeszka, A. Sroczynska, R. Wojciechowski, J. Ulanski, V. Laukhin, *Synth. Met.* **1999**, *102*, 1785.

[6] a) J. M. Williams, J. R. Ferraro, R. J. Thorn, K. D. Carlson, U. Geiser, H. H. Wang, A. M. Kini, M.-H. Whangbo, *Organic Superconductors (Including Fullerenes): Synthesis, Structure, Properties and Theory*, Prentice Hall, Englewood Cliffs, NJ **1992**. b) J.-P. Farges, *Organic Conductors, Fundamentals and Applications*, Marcel Dekker, New York **1994**.

[7] J. Ulanski, A. Tracz, J. K. Jeszka, E. Laukhina, A. Khomenko, P. Polanowski, D. Staerk, H. W. Helberg, in *NATO ARW: Electrical and Related Properties of Organic Solids* (Eds: R. W. Munn, B. Kuchta, A. Miniewich), Kluwer, Dordrecht, The Netherlands **1996**, p. 241.

[8] P. W. Atkins, *Physical Chemistry*, Oxford University Press, Oxford **1978**.

[9] X-ray diffraction patterns were measured on a Siemens-D500 diffractometer in the reflection θ–2θ mode using Cu Kα_1 radiation.

[10] NIR spectra were recorded using a Varian Cary05E spectrophotometer.

[11] J. B. Torrance, B. A. Scott, B. Welber, F. B. Kaufmann, P. E. Seiden, *Phys. Rev. B* **1979**, *19*, 730.

[12] The morphology of the conducting surface layers was investigated using a scanning electron microscope operating at 20 kV.

  1616-301X/01/0408-0303 $ 17.50+.50/0

COMUNICACIÓ F

Títol: Synthesis Improvement, Crystal Structure and a Charge-Transfer Complex of a Sulphur Dioxide-Containing TTF Derivative.

Autors: M. Mas-Torrent, J. Llacay, K. Wurst, V. Laukhin, J. Vidal-Gancedo, J. Veciana and C. Rovira.

Publicació: *Synth. Met*., 128, 157-161.

Any: 2002

ARTICLE G

Títol: New molecular charge transfer salts of TM-TTF and BMDT-TTF with thiocyanato- and selenocyanato-complex anions; TMTTF = tetramethyltetrathiafulvalene, BMDT-TTF = bis(methylenedithio)-tetrathiafulvalene.

Autors: M. Mas-Torrent, S. S. Turner, K. Wurst, J. Vidal-Gancedo, J. Veciana, C. Rovira, P. Day.

Publicació: *J. Mater. Chem., enviat*.

ARTICLE H

Títol: Two New Families of Charge Transfer Solids Based on $[M(mnt)_2]^{n-}$ and the Donors BMDT-TTF and EDT-TTF. Conducting and Magnetic Properties.

Autors: M. Mas-Torrent, H. Alves, E. B. Lopes, M. Almeida, K. Wurst, J. Vidal-Gancedo, J. Veciana and C. Rovira.

Publicació: *J. Solid State Chem*., enviat.

ARTICLE I

Títol: Electronic Localization in An Extreme 1-D System: The New Charge Transfer Salt (TTDM-TTF)$_2$[Au(mnt)$_2$].

Autors: E. B. Lopes, H. Alves, E. Ribera, M. Mas-Torrent, P. Auban-Senzier, E. Canadell, R. T. Henriques, M. Almeida, E. Molins, J. Veciana, C. Rovira, D. Jérome.

Publicació: *Eur. Phys. J. B*., enviat.

ARTICLE J

Títol: New Molecular Conductors Based on ETEDT-TTF Trihalides: From Single Crystals to Conducting Layers of Nanocrystals.

Autors: M. Mas-Torrent, E. Ribera, V. Tkacheva, I. Mata, E. Molins, J. Vidal-Gancedo, S. Khasanov, L. Zorina, R. Shibaeva, R. Wojciechowski, J. Ulanski, K. Wurst, J. Veciana, V. Laukhin, E. Canadell, E. Laukhina and C. Rovira.

Publicació: *Chem. Mater.,* en premsa.

CAPÍTOL DE LLIBRE K

Títol: Stability of the Metallic State in New Hydrated Molecular Metals: $(BET\text{-}TTF)_2X\cdot 3H_2O$.

Autors: E. Laukhina, A. Pérez-Benítez, M. Mas-Torrent, E. Ribera, C. Rovira, J. Veciana, J. Vidal- Gancedo, V. Laukhin.

Publicació: *Molecular Low Dimensional and Nanostructured Materials for Advanced Applications (MMAA)*. Editor: Prof. A. Graja, en premsa.